Title

Modeling the direct sun component in buildings using matrix algebraic approaches: Methods and validation

Authors

Lee, Eleanor S
Geisler-Moroder, David
Ward, Gregory

Publication Date

2018

DOI

10.1016/j.solener.2017.12.029

Peer reviewed

LBNL- 2001102

BERKELEY LAB

Lawrence Berkeley National Laboratory

Modeling the direct sun component in buildings using matrix algebraic approaches: Methods and validation

Eleanor S. Lee[a]*, David Geisler-Moroder[b], Gregory Ward[c]

[a] Building Technologies and Urban Systems Division, Energy Technologies Area, Lawrence Berkeley National Laboratory, Mailstop 90-3111, 1 Cyclotron Road, Berkeley, California 94720 USA

[b] Bartenbach GmbH, Rinner Str. 14, 6071 Aldrans, Austria

[c] Anyhere Software, 950 Creston Road, Berkeley, California, 94708 USA

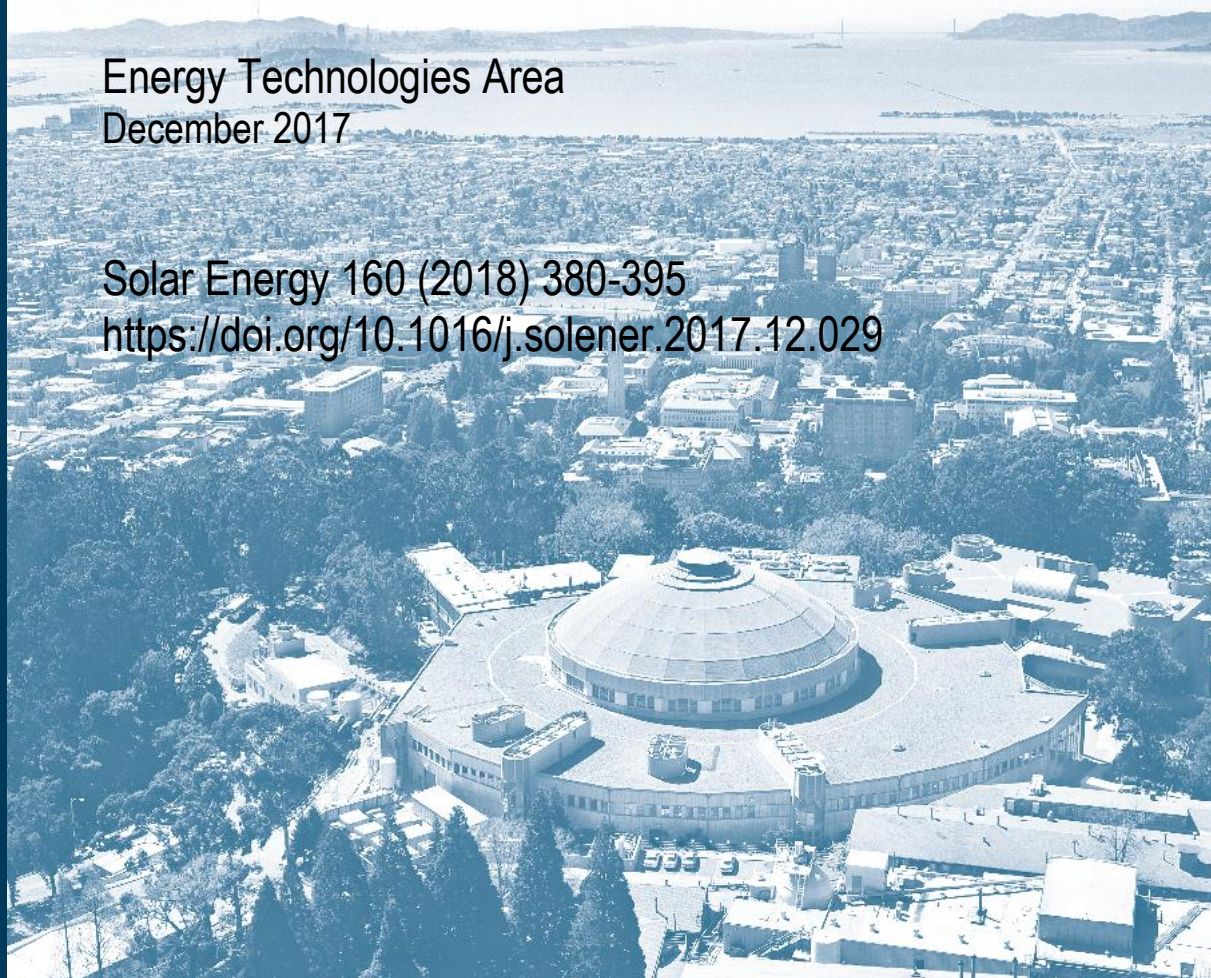

Energy Technologies Area
December 2017

Solar Energy 160 (2018) 380-395
https://doi.org/10.1016/j.solener.2017.12.029

Disclaimer

Acknowledgments

This work was supported by the Assistant Secretary for Energy Efficiency and Renewable Energy, Building Technologies Program of the U.S. Department of Energy under Contract No. DE-AC02-05CH11231, by the California Energy Commission through its Electric Program Investment Charge (EPIC) Program on behalf of the citizens of California, by Pacific Gas and Electric Company's Emerging Technologies Program, and by the Austrian Research Promotion Agency (FFG) through the "lightSIMheat" project under Contract No. 838718. In-kind support was provided by Lucent Optics, Serralux, and SmartLouvre.

Amir Roth, U.S. Department of Energy, and Dustin Davis, California Energy Commission, provided invaluable support over the term of this research. We would also like to acknowledge the contributions of Wilfried Pohl and Christian Knoflach, Bartenbach GmbH, and LBNL team members Taoning Wang, Anothai Thanachareonkit, Jacob Jonsson, Christoph Gehbauer, Darryl Dickerhoff, Jordan Shackelford, Daniel Fuller, Ari Harding, Cynthia Regnier, and Stephen Selkowitz. Andrew McNeil and Christian Humann, Terrestrial Light, provided additional technical support related to the field validation.

Solar Energy 160 (2018) 380-395

Modeling the direct sun component in buildings using matrix algebraic approaches: Methods and validation

Eleanor S. Lee[a*], David Geisler-Moroder[b], Gregory Ward[c]

[a] *Building Technologies and Urban Systems Division, Energy Technologies Area, Lawrence Berkeley National Laboratory, Mailstop 90-3111, 1 Cyclotron Road, Berkeley, California 94720 USA*
[b] *Bartenbach GmbH, Rinner Str. 14, 6071 Aldrans, Austria*
[c] *Anyhere Software, 950 Creston Road, Berkeley, California, 94708 USA*

Abstract

Simulation tools that enable annual energy performance analysis of optically-complex fenestration systems have been widely adopted by the building industry for use in building design, code development, and the development of rating and certification programs for commercially-available shading and daylighting products. The tools rely on a three-phase matrix operation to compute solar heat gains, using as input low-resolution bidirectional scattering distribution function (BSDF) data (10-15° angular resolution; BSDF data define the angle-dependent behavior of light-scattering materials and systems). Measurement standards and product libraries for BSDF data are undergoing development to support solar heat gain calculations. Simulation of other metrics such as discomfort glare, annual solar exposure, and potentially thermal discomfort, however, require algorithms and BSDF input data that more accurately model the spatial distribution of transmitted and reflected irradiance or illuminance from the sun (0.5° resolution).

This study describes such algorithms and input data, then validates the tools (i.e., an interpolation tool for measured BSDF data and the five-phase method) through comparisons with ray-tracing simulations and field monitored data from a full-scale testbed. Simulations of daylight-redirecting films, a micro-louvered screen, and venetian blinds using variable resolution, tensor tree BSDF input data derived from interpolated scanning goniophotometer measurements were shown to agree with field monitored data to within 20% for greater than 75% of the measurement period for illuminance-based performance parameters. The three-phase method delivered significantly less accurate results. We discuss the ramifications of these findings on industry and provide recommendations to increase end user awareness of the current limitations of existing software tools and BSDF product libraries.

Keywords: daylighting; bidirectional scattering distribution function (BSDF); validation; building energy simulation tools; solar heat gains; windows.

1. Introduction

Window shades, films, and other types of "attachments" have significant potential to reduce energy consumption in residential and commercial buildings through rejection or admission of solar heat gains and

* Corresponding author, Tel.: +1 510 486 4997. E-mail address: eslee@lbl.gov (E.S. Lee).

daylight and improvements to the thermal properties of the window. Such systems are estimated to have a technical potential to save 1.0-2.8 EJ (0.98-2.62 quads, where 1 quad = 10^{15} Btu) annually in energy use in the U.S. compared to the current building stock [Arasteh et al. 2006]. There has been considerable interest in fenestration attachments recently because they can reduce the energy use of existing buildings cost effectively in the near-term [Lee et al. 2009, DOE 2014]. In 2014, the U.S. Department of Energy (DOE) initiated an industry-led program to develop a rating and certification program for residential window attachments. Providing third-party information to the consumer for more informed purchasing decisions is an effective strategy for increasing market adoption of energy-efficiency technologies. The resultant Attachments Energy Rating Council (AERC) developed a rating and labeling scheme that reflects annual heating and cooling energy use in residential buildings [AERC 2017]. A similar rating and certification program is planned for commercial buildings. In Europe, the European Solar-Shading Organization (ES-SO) is also working to develop a rating and certification program for window attachments [ES-SO 2017].

For these and other related market pull activities, simulation models and input data are needed to quantify the impact of light scattering or "optically-complex" fenestration systems on heating, ventilation, and air-conditioning (HVAC) energy use, lighting energy use, comfort, and indoor environmental quality. Algorithm development and measurement protocols for characterizing the angle-dependent solar-optical properties of static and operable complex fenestration systems have been under development worldwide for some time, particularly with respect to solar heat gains. These algorithms model solar irradiance contributions from the sun and sky to the room interior by subdividing the skydome hemisphere into a grid of large-area patches (10-15° angular resolution) then integrating the irradiance contributions from the subdivided sky to derive total incoming radiation through the fenestration system. Simulation of other metrics such as discomfort glare, daylighting, and those related to thermal comfort if the subject is irradiated, however, require algorithms that more accurately model the spatial distribution of transmitted and reflected irradiance from direct sunlight within the room interior.

The objective of this study is to explain the differences in methods and accuracy when modeling the effects of direct sunlight using a matrix algebraic approach, specifically for daylighting applications of optically-complex fenestration systems (CFS). Section 2 describes the modeling approaches for evaluating solar heat gains and daylighting. Section 3 describes how angle-dependent BSDF properties are measured and/or simulated to support daylighting applications. Section 4 describes the results of validation studies that 1) estimate the error associated with interpolated measured BSDF data, 2) assess the accuracy of the entire modeling work flow (algorithms, input data, interpolation tools) using measured data from an outdoor full-scale testbed, and 3) isolate errors from the three- and five-phase matrix algebraic methods through comparisons with ground truth ray-tracing calculations. Ramifications on industry activities related to design, product development, and rating and certification activities are discussed with suggestions for future work.

2. Modeling daylight performance using a matrix algebraic approach

In 1994, Klems proposed a time-efficient method for determining solar heat gains through complex fenestration systems [Klems 1994a,b]. The matrix algebraic method achieved a practical balance between time-consuming calorimetric measurements and first principle calculations, enabling accurate building energy performance evaluations in a fraction of the time needed by prior methods. The method relies on angle-dependent transmittance and reflectance or "scattering" measurements for each layer of the fenestration system. The properties of multi-layered fenestration systems (consisting of parallel glazing and shading layers) are built up computationally from individual measured layer properties using a transmission and multiple reflection calculation. The resultant bidirectional scattering distribution functions (BSDF) or angle-dependent luminous coefficients for a given incident angle (Figure 1) are

multiplied by the incident irradiance from each grid element of the incoming hemisphere, then summed to obtain total outgoing transmitted irradiance into the room. The direct-hemispherical transmission for incident direction (θ_1,ϕ_1) is thus given by:

$$\tau(\theta_1,\phi_1) = \int_0^{2\pi}\int_0^{\pi/2} BTDF(\theta_1,\phi_1,\theta_2,\phi_2)\cos\theta_2 \sin\theta_2 \, d\theta_2 \, d\phi_2 \tag{1}$$

with integration of irradiance over all directions (θ_2,ϕ_2) in the outgoing scattering hemisphere. In Equation 1, θ and φ define the boundaries of each grid element or "patch" of the hemispherical basis (Figure 1). Or more simply:

$$\tau(patch_i) = \sum_{k=1}^{145} BTDF(patch_i, patch_k)\,\Omega_k \tag{2}$$

Equation 2 shows the integration of flux over the Klems BTDF hemispherical basis (145 incoming and 145 outgoing grid elements), where Ω_k is the projected solid angle for the k^{th} patch of the basis. A layer-by-layer matrix calculation is done using a similar approach in order to determine absorbed and inward-flowing solar radiation from the fenestration system. The sum of the transmitted and absorbed and inward flowing fraction of radiation equals the total solar heat gain from the fenestration system.

Note that the subdivision of the hemisphere into a grid of solid angles, known as the directional "basis", is defined for different purposes. Klems, for example, modified the Tregenza (sky) hemispherical subdivision for the purpose of solar heat gain calculations, giving higher resolution in incident angle and a weighting of the patches proportional to their solid angle and projected area. The angular resolution of this basis is approximately ±5° in incident angle and much coarser in azimuth. Other bases developed for daylighting applications are listed in Section 3.

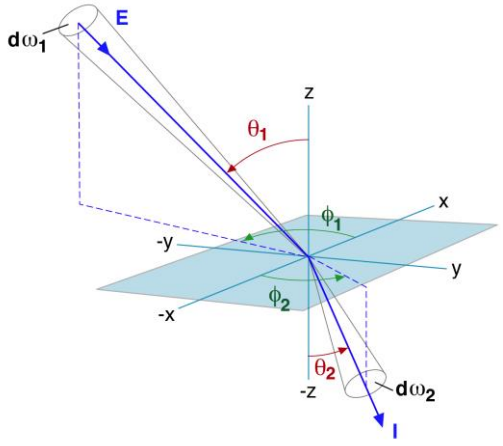

Figure 1. Incoming and outgoing angles relative to the sample material (shown as a blue plane).

Between 2011 and 2014, Klems and others at the Lawrence Berkeley National Laboratory (LBNL) modified the WINDOW and EnergyPlus simulation tools to incorporate Klems' approach for calculating solar heat gains, resulting in new releases of the software tools WINDOW 7 [2017] and EnergyPlus 8.1 [2017].

2.1. Modeling daylight using the three-phase method

In 2006, Ward adapted the Klems matrix algebraic approach to enable computation of annual daylighting performance in interior spaces using Radiance [Ward Larson and Shakespeare 1998, Saxena et al. 2010, Ward et al. 2011]. This "three-phase" matrix approach (Equation 3), which was a variant on [Tregenza and Waters 1983] then Reinhart and Herkel's earlier daylight coefficient (dc) approach [Reinhart and Herkel 2000, Reinhart and Walkenhorst 2001], incorporates the BSDF matrix ("T") representing the fenestration system:

$$\mathbf{E} = \mathbf{VTDS} \tag{3}$$

where,

- **E** is the resulting annual series of the desired illuminance (or luminance, L) at a specified location in the interior space;
- **S** is the sky matrix, representing the luminance of the subdivided sky hemisphere, including the orb of the sun for the overall year;
- **D** is the daylight matrix, which relates the flux transfer between the sky hemisphere and the outdoor surface of the window/ fenestration system;
- **T** is the transmission matrix or BSDF for the fenestration system, which relates the incident flux on the fenestration system to the outgoing exiting flux from the fenestration system into the room; and,
- **V** is the view matrix, which relates the flux transfer between the fenestration system and the specified location in the interior.

Like the Klems approach for computing solar heat gains, this approach enables efficient modeling of operable shading and daylighting systems (e.g., roller shades, venetian blinds, etc.) through the interchange of the BSDF matrix without the necessity of recomputing the other two matrices. This method enables analysis of annual performance within a fraction of the time it took using conventional ray-tracing methods, opening the door for accelerated technological development and design analysis using optimization algorithms and parametric analysis.

Fundamental limitations of the three-phase method were discussed in [Ward et al. 2011; McNeil and Lee 2012]. Errors in both spatial distribution and intensity of flux within the modeled interior space are introduced when a continuous relationship is represented by a discrete set of data in the matrix formulation (i.e., luminance distribution over the skydome hemisphere (**S** matrix), patterns of light transmission over the outgoing hemisphere (**T** or BSDF matrix)). (1) The Klems BSDF basis divides the incoming and outgoing transmittance and reflectance hemispheres into 145 grid elements or patches with an average solid angle of 0.043 steradians per subdivision or a cone with a 13.5° apex angle (the solar orb has a 0.5° apex angle). With the calculation of solar heat gains, this resolution is sufficient to produce accurate results. For daylight parameters, alternate BSDF basis definitions have been defined (see Section 3) [Aydinli and Kaase 1999; de Boer 2005; Kämpf and Scartezzini 2011]. (2) For the sky matrix, Tregenza defined an angular basis for subdivision of the skydome hemisphere into 145 solid angles [Tregenza 1983]. Here, the radiance of the sun orb can be spread out over as many as three sky subdivisions, depending on the position of the sun orb in the sky for a specific time of day. In the mapping of the Tregenza sky matrix to the Klems (window) BSDF, the sky subdivisions do not align with the Klems subdivisions. As a result, solar radiation can also be spread over as many as six Klems patches. On the interior, the resultant transmitted radiation has a reduced intensity and is spread out over a larger area in the interior space than would otherwise occur if the angular resolution of the sky subdivisions and BSDF basis were made more granular.

To address the source of error related to the 145 sky subdivisions, the sky hemisphere can be uniformly subdivided into smaller solid angles to more closely model the solid angle of the sun orb. The Tregenza angular basis subdivided by a factor of four (Reinhart MF:4) results in a total of 2305 subdivisions or a 3° apex angle [Jakubiec and Reinhart 2011]. If the sun position results in the sun's radiation being assigned to adjacent patches, then the apex angle is effectively doubled. If the basis subdivided by a factor of 16 is used to achieve a 1.5° resolution or 36,866 sky patches, the Windows operating system (used by most building engineers) with an open file limit of 2048 causes the program to abort[1]. The BSDF resolution could also be increased by subdividing the Klems basis into smaller solid angles, as suggested in Ward et al. 2011. In both cases, increasing resolution increases the amount of time it takes to both generate the initial matrices and then to perform the matrix multiplication step for the annual simulation.

2.2. Modeling daylight using the five-phase method

A pilot study was conducted to examine the change in annual lighting energy and visual discomfort performance when the resolution of the BSDF basis (number of hemispherical subdivisions) was increased by a factor of four and used with the three-phase method [McNeil 2011]. Results showed that there was a minimal effect on annual lighting energy use since ceiling-mounted photosensor-based control effectively averages out local non-uniformity from sunlight on work surfaces. BSDF resolution did however have a significant effect on the annual assessment of discomfort glare – discomfort glare was estimated to occur more frequently – an additional 7% of the year – when BSDF input data with the Klems basis (145×145) was used instead of the Klems basis subdivided by a factor of four.

To improve accuracy, McNeil and others[2] proposed an alternate five-phase method to the three-phase method (Equation 4) where the direct sun and diffuse sky contributions are calculated separately [McNeil 2013]. The diffuse sky's contribution to interior illuminance or luminance is computed with the Tregenza sky (145 subdivisions) and the Klems BSDF basis (145×145 matrix) in the same manner as the original three-phase method. The direct sun's contribution is separately computed using the intensity of the sun with its actual solid angle (calculated for a grid of points over the skydome hemisphere) so that its flux is no longer spread out over corresponding sky patch(es) (Figures 2-3). The fenestration system is represented by its geometry if possible, or by BSDF data with a variable resolution, tensor tree angular basis (see Section 3). For a tensor tree BSDF basis resolution equal to an apex angle of no smaller than 3° for example, the 0.5° orb of the sun is spread out by a square of that ratio, or is about a factor of 36 less bright than it would be in reality if unscattered. By separating the direct and mirror components from the diffuse component, the spatial distribution of solar intensity is represented more accurately. This method could improve the prediction accuracy of performance parameters beyond just daylighting in cases where accurate distribution of solar intensity is important.

$$\mathbf{E} = \mathbf{VTDS} - \mathbf{V}_d\mathbf{TD}_d\mathbf{S}_{ds} + \mathbf{C}_{ds}\mathbf{S}_{sun} \quad (4)$$

where,

- **E**, **S**, **T**, **D**, and **V** are as described in Equation 3;
- $\mathbf{S}_{ds}$ is the sky matrix for the direct sun component for the overall year, calculated using the three-phase method; in this matrix only the Tregenza sky patch(es) representing the sun orb are nonzero;

[1] The default of 512 open files under the Windows operating system can be increased by the end user to 2048 [Microsoft 2017] but this limit is still insufficient for the desired level of accuracy.

[2] A. McNeil (LBNL), R. Guglielmetti (National Renewable Energy Laboratory), R. Mistrick (Pennsylvania State University), and G. Ward (Anyhere Software) conceived of the five-phase method in a 2012 meeting at LBNL.

– $\mathbf{D}_d$ is the daylight matrix for the direct sun component, calculated using the three-phase method; it represents the flux transfer between the sun and fenestration system without interreflections from the ground or other surrounding outdoor surfaces;
– $\mathbf{V}_d$ is the view matrix for the direct sun component, calculated using the three-phase method; it represents the flux transfer between the fenestration system and the specified location in the interior from direct sun without interreflections from the room interior;
– $\mathbf{S}_{sun}$ is the direct sun matrix, representing the luminance of the sun orb for the same grid of positions in the skydome hemisphere for the overall year; and,
– $\mathbf{C}_{ds}$ is the coefficient matrix relating the flux transfer from the sun orb for a grid of positions in the skydome hemisphere to a specified location in the interior without interreflections; the variable resolution, tensor tree BSDF of the fenestration system (with or without proxy geometry) is included in the calculation of the $\mathbf{C}_{ds}$ matrix.

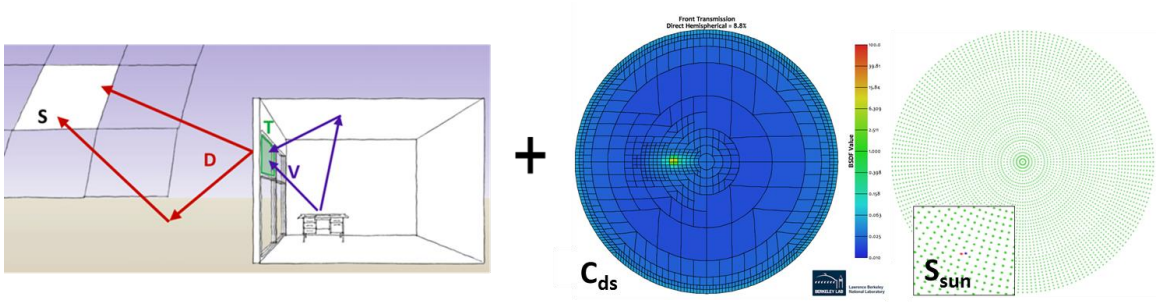

Figure 2. Graphic showing the sky (left) and sun (right) contributions to a point location in the indoor space with the associated matrices for the five-phase method.

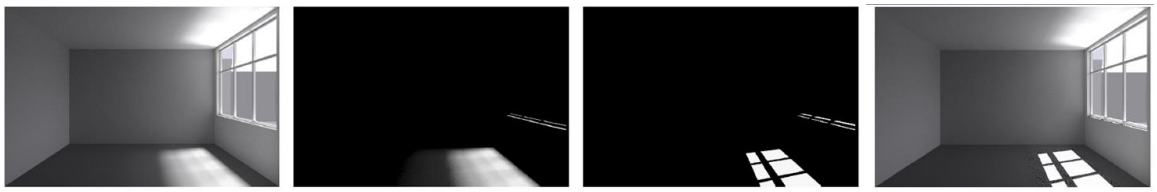

L_{3pm} $- L_{ds\text{-}3pm}$ $+ L_{ds}$ = L_{5pm}

Figure 3. Renderings of the luminance (L) contributions in an indoor space with clear glazing. Results from the three-phase method (L_{3pm}, left hand image), minus the contribution from the sun patches from the three-phase method ($- L_{ds\text{-}3pm}$), plus the contribution from the orb of the sun ($+ L_{ds}$), equals the result from the five-phase method (L_{5pm}, right hand image). Note how the sunlit areas are rendered with greater spatial accuracy with the five-phase method. Image from [McNeil 2013].

2.3. Refinements to the five-phase method

Geisler-Moroder et al. [2017] completed a preliminary validation study comparing field measured data to simulated data generated using the five-phase method. As a result of the study, the five-phase method was further refined to include the luminance of the shading system itself ($\mathbf{C}_{F\text{-}ds}$), improving the accuracy of the luminance calculation (rendered images), and calculation of visual discomfort.

$$\mathbf{L} = \mathbf{VTDS} - \mathbf{V}_d\mathbf{TD}_d\mathbf{S}_{ds} + (\mathbf{C}_{R\text{-}ds} + \mathbf{C}_{F\text{-}ds})\,\mathbf{S}_{sun} \quad (5)$$

where,

- **L**, all matrices in the first and second terms, and $\mathbf{S}_{sun}$ are as described in Equation 4;
- $\mathbf{C}_{R\text{-}ds}$ is the same coefficient matrix as $\mathbf{C}_{ds}$ in Equation 4 (renamed to differentiate it from the façade-side coefficient matrix); and,
- $\mathbf{C}_{F\text{-}ds}$ is the façade-side coefficient matrix relating the flux transfer from the sun orb for a grid of positions in the skydome hemisphere to the luminance as seen at the façade itself without interreflections from the outdoors or indoors but inclusive of the contributions of direct sun on and interreflected within the fenestration system itself; variable BSDF data or the geometry of the system is also included in this calculation.

The direct sun coefficient matrix $\mathbf{C}_{ds}$ in Equation 4 is thus replaced by the sum of two coefficient matrices for the direct sun contribution inside the room $C_{R\text{-}ds}$ and the direct sun contribution seen at the façade $C_{F\text{-}ds}$. This modification is necessary to account for an improved representation of the direct sun contribution to the luminance at the fenestration system itself.

Conceptually, the five-phase method is similar to the four component approach proposed by [Mardaljevic 2000], which separates direct and indirect illuminance from the sun and from the sky as a variant of the direct coefficient approach. The five-phase method however loses some of its key advantage of efficient modeling of parameterized or operable fenestration systems through simple exchange of the **T** BSDF matrix. This is due to the introduction of the third term in Equations 4 and 5, which requires a full ray-tracing calculation (albeit without ambient bounces) that includes a *fixed* BSDF for the fenestration system for each sun position. Also, because of limitations with the Radiance tools when computing the second term in Equation 4, all interior surfaces are modeled as Lambertian (hemispherically diffusing) so specular reflections from direct sunlight are not included in this part of the calculation and are thus represented as in the three-phase method. Trade-offs in accuracy and computational speed between the five-phase method and other modeling approaches (e.g., direct coefficient or two-phase method with a high-resolution sky basis) should be investigated further. The five-phase method may very well retain its advantage of high computational speed over the daylight coefficient method and greater accuracy for operable and parametric fenestration applications.

3. Generating BSDF data for specularly transmitting materials and systems

Daylight calculations using the three- and five-phase methods require angle-dependent BSDF data as inputs. To address the five-phase method's need for high directional data resolution with a compact data structure, a BSDF dataset with an adaptive or variable resolution basis was developed [Ward et al. 2012, Geisler-Moroder 2011]. This "tensor tree" basis provides high angular resolution (e.g., 1.5° apex angle) in areas of peak transmission and low resolution (10-15° apex angles) in areas where more diffuse transmission occurs. This section discusses how BSDF data for a single fenestration layer are generated from measured data, ray-traced geometric models, models derived from measured data or other means. The section focuses on BSDF generation methods for "peaky" fenestration layers (i.e., with a specular transmission component).

As discussed in Section 2, the Klems matrix algebraic method was designed to enable modeling of any arbitrary *multi-layered* fenestration systems, given the infinite number of combinations possible with glazing and shading layers. The tensor tree basis presents a difficult challenge to this initial concept because of its variable rather than fixed resolution basis definition. However, an innovative method was developed recently to combine tensor tree BSDF data from multiple coplanar layers into a single BSDF, requiring a fraction of the time to produce BSDFs compared to a conventional ray-tracing approach [Grobe 2017a].

For reference, basis definitions for both the skydome and fenestration BSDFs are summarized in Table 1.

Table 1. Hemispherical bases for the sky and transmission matrices

Name	Description	Matrix	Number of subdivisions	Min. angular resolution (º)
Tregenza	Subdivision of the skydome	**S**	145	10-15º
Reinhart (MF:N)	Tregenza basis; each grid element subdivided by a factor of N^2	**S**	MF:2 = 577 MF:4 = 2305	6º 3º
Klems	BSDF for solar heat gains	**T**	145×145	10-15º
IEA SHC Task 21	BSDF for daylighting	**T**	145×1297	10-15° incident and 5° exiting
Tensor tree (TT)	Variable-resolution BSDF for daylighting	**T**	$2^{2\cdot k} \times 2^{2\cdot k}$ then reduced to a 4-dimensional compact tensor tree structure	For k=3-7,[3] resolution varies from 20°-1.5º

3.1. Angle-dependent transmittance and reflectance measurements

Measuring the *peak* intensity and angular distribution of transmitted, reflected, or redirected radiation is one of the key challenges of characterizing optically-complex fenestration systems. Measuring strong localized peaks requires an instrument with a narrow beam diameter, broad dynamic measurement range, and sufficiently fine angular resolution of the measurements, particularly in the outgoing scattering direction [Apian-Bennewitz and von der Hardt, 1998; Andersen and de Boer, 2006; Andersen et al. 2010; Apian-Bennewitz 2010]. Measurement systems developed over the past few decades, however, were designed for different objectives and therefore with different levels of resolution. Stover [1995] provides a comprehensive resource for measurement and analysis of optical scattering, including effects of instrumentation on the averaged BSDF measurement. Schwanengel [2010] compared the measurable contrast (dynamic range) and angular resolution between various instruments. Scanning goniophotometers yielded a contrast of greater than 1:20,000 and an angular resolution better than 0.04° with 0.01° step size depending on sensor size and distance to the sensor. Ulbricht imaging spheres yielded a contrast of less than 1:200 and an angular resolution of 0.5°. Andersen et al. [2005a] indicated a sampling resolution of greater than 100,000 points per hemisphere for the scanning goniophotometer and 1297 points per hemisphere for an imaging goniophotometer. Grobe et al. [2010] conducted a round robin comparison on three sample materials and identified sources of error that contributed to differences in measurements between the three participating institutions when using the same type of scanning goniophotometer. Krehel et al. [2015] compared the measured BSDF data of several sample daylight redirecting materials and found that the larger beam diameter and lower resolution of acquired data from an imaging goniophotometer led to greater spread in light scattering properties, causing significant dissimilarities with a high resolution

[3] It is possible to generate BSDFs to a resolution of k=10 using a function and *bsdf2ttree* if the material is isotropic (i.e., –t3 10). For anisotropic materials, k=10 is not possible due to memory limitations (only –t4 7 is possible at this time).

scanning goniophotometer. Research to be conducted in the International Energy Agency Solar Heating and Cooling Program Task 61is intended to establish BSDF measurement standards for the daylighting community [de Boer 2017] as a follow on activity to Task 50 [Kämpf et al. 2016].

Another challenge is obtaining complete characterizations when measured data are missing (when the goniophotometer blocks the light source) or sampling is sparse. Measurements for a single incident direction can take a few seconds with an imaging goniophotometer or a few minutes with a scanning goniophotometer, not including set up time. For the Klems basis, measurement of all 145 incident directions can take an appreciable amount of time, particularly if additional high resolution scanning is conducted where peaks occur. Symmetry within the material or system can reduce the required number of incident angles. For an isotropic material, nine incident directions (one ϕ angle, nine θ angles) may be sufficient. For asymmetric, anisotropic materials, all 145 incident directions must be measured. For partial measured data sets, interpolation tools are needed to generate complete BSDF data sets for all required incident and outgoing angles. A tool developed for this purpose is described in Section 3.3.

3.2. Generating BSDFs

3.2.1. Generating BSDFs using a geometric model and material properties

Ray-tracing tools such as TracePro (Lambda Research Corporation) can be used with a geometrical description of the fenestration system and hypothetical or actual measurements of material properties to produce complete BSDF data sets [Andersen et al. 2005b]. Use of such tools may be the only option in cases where the material properties or fenestration system has a scale that is too large to be measured within the narrow beam diameter of the goniophotometer (e.g., repeating elements of a louver system). An open source, ray-tracing tool called *genBSDF* [Radiance 2010] was developed for this purpose and validated using simulated and field measured data [McNeil et al. 2013, Molina et al. 2015]. *genBSDF* uses a geometric model and transmittance and/or reflectance properties of the basic materials that make up the fenestration system to generate a full BSDF. Plastics, glass, metals, and other materials are defined by Radiance primitives. Measured BSDF materials can also be specified using the Radiance "BSDF material" type.

To determine the direct sun contribution using the five-phase method (third term in Equation 4), two methods can be used to generate the direct sun coefficients C_{ds}: 1) a variable-resolution tensor tree BSDF data set can be used or, 2) one can apply ray-tracing using the detailed geometry of the fenestration system, if the geometry is available to the end user. With the former method, a tensor tree BSDF data set with a 3º resolution ($2^{2\cdot6}$ x $2^{2\cdot6}$ or –t3 6 in the Radiance command language) still produces blurry edged shadows when modeling a system with distinct edges, like a venetian blind. With the latter method, view rays interact with the geometry of the venetian blinds, as do rays sent to test for light sources and shadows – there is no reliance on BSDF sampling parameters so the spatial distribution for the direct sun contribution is absolutely accurate (e.g., sharp edged, striped shadow pattern for venetian blinds).[4] The *genBSDF* tool provides a facility to transfer the geometric model to a special tag in the XML output file, where it may later be used for shadow ray testing and correct system appearance when the window is in the field of view. With the calculation of the diffuse sky contribution (the first two terms of Equation 4), indirect sampling rays interact only with "proxy" surfaces represented by the Klems BSDF [Ward et al. 2012]. Indirect sunlight originating from inside the geometry of the venetian blinds are ignored by the proxy surface and care must be taken to avoid double counting the unscattered transmission from the sun. In Geisler-Moroder

[4] In general, this method of embedding geometry in the BSDF description supports more accurate renderings, the daylight coefficient method, and the five-phase method but not the three-phase method.

[2017], additional modifications were made to *Radiance* after completion of the preliminary validation study to more accurately represent the contributions from the sun orb. Because standard Monte Carlo sampling methods cannot find small, bright sources, special tests were added for systems with a strong "view" component. Specifically, shadow testing, the practice of sending carefully aimed rays towards light sources, was made to work through BSDFs with strong view components.

Variations in a manufactured product can increase the complexity of BSDF characterization when either the measured or synthetic approach is used. In Noback et al. [2016], a forward ray-tracing algorithm implemented in a photon map extension to Radiance [Schregle et al. 2015] was used to generate BSDF data for a complex louver system involving highly reflective surfaces. The study proposed two metrics for characterizing the variation in BSDF data given manufacturing deviations from the design geometry. In McNeil et al. [2017], synthetic BSDF data sets were first derived from profiles drawn from electron microscope scans of fabricated microprismatic structures, then these data sets and a BSDF data set derived from the original design were averaged for each paired incident and outgoing direction to better match the characteristics of the manufactured product. Research is needed to develop characterization methods for products that exhibit variability in both geometry and/or optical properties.

3.2.2. Generating BSDFs from models

BSDF datasets can also be generated using models derived from detailed measurements. This is particularly useful for materials or systems where ray-tracing models are inadequate and comprehensive goniophotometer measurements for each variation of the system are deemed impractical. Fabric roller shades is an example of where such models may be useful – there are thousands of design permutations of weave and color available on the market and designs can change from year to year. A simple geometric model may inadequately represent the light-scattering and transmitting properties of the thread and variations in weave needed for daylighting performance evaluations. Kotey [2009] and Jonsson et al. [2015] derived analytical models for roller shade fabrics based on angle-tube measurements of total and diffuse transmittance using a spectrophotometer. Instead of measurements for the requisite 81or so angles of incidence needed for an asymmetric sample with left-right hand symmetry, these models generate BSDF datasets for solar heat gain evaluations from a single measurement at normal incidence. Use of the Kotey BSDF dataset with a hybrid ray-tracing and radiosity simulation tool was shown to have good agreement with measured workplane illuminance data [Tzempelikos and Chan 2016]. Accuracy of the model for discomfort glare evaluations was not assessed against measured data or a more accurate modeling approach (e.g., full ray-tracing). Development of analytic or empirically-derived models for daylighting performance parameters such as discomfort glare will require careful validation and testing. Such models will need to accurately replicate the angle-dependent peaky light-scattering behavior of the fenestration system.

3.3. Interpolation tool for data-driven BSDFs

For the cases where the system or material BSDF cannot be generated based on a geometric model (as in Section 3.2.1.) or analytic model (as in Section 3.2.2), an interpolation tool *pabopto2bsdf* [5]was developed to generate BSDF data from sparse scanning goniophotometer measured data for incident angles for which there are no measurements. The interpolation tool uses a generalized three-way displacement interpolation method similar to [Bonneel et al. 2011] and described in [Ward et al. 2012, 2014]. The peaky aspects of the fenestration system are represented using a series of radial basis functions and interpolated using a cost

[5] There is yet no manual documentation for these tools because there are less than a handful of institutions in the world with the pgII Apian Bennewitz scanning goniophotometer (http://www.pab.eu/). The code is open source and available at the Radiance website (https://radiance-online.org//).

function based on Earth Mover's Distance. *bsdf2klems* and *bsdf2ttree* are then used to convert the scattering interpolants into the requisite BSDF representations with Klems and tensor tree bases, respectively. In the latter, the subprogram *rttree_reduce* is responsible for reducing the full matrix into a sparse structure by merging similar neighboring values.

The steps for the overall procedure are as follows:
Step 1: Organize the BSDF measured data based on incident and outgoing (scattering) hemispheres.

Step 2: For each measured incident direction, a Radial Basis System (RBS), which is a collection of 50 to 200 Gaussian lobes, is fit to the measured outgoing, scattering data. Each Gaussian lobe has a central direction, a peak value, and a half-maximum angle. The lobes should sum to a reasonable representation of the measured data, with some smoothing of the data applied to fill gaps and reduce noise in the measurements (Figure 4).

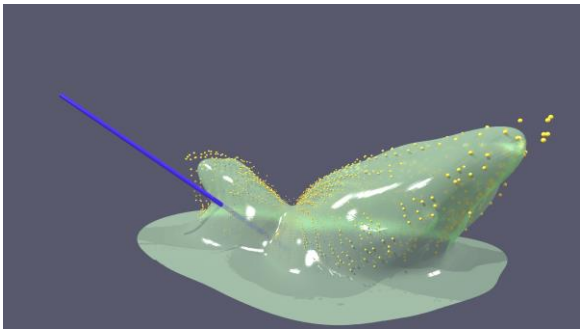

Figure 4. Interpolation of measured outgoing scattering values for a single incident direction, shown as blue line. Yellow dots are measurements, and green surface is interpolation using radial basis functions.

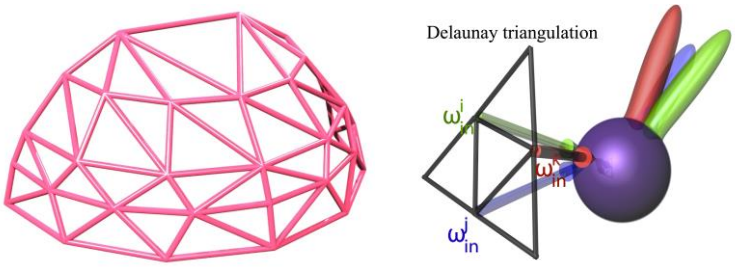

Figure 5. Left: Delaunay mesh connecting incident directions (vertices) on half-hemisphere. Right: Geometry used for interpolating incident directions between Delaunay vertices.

Step 3: All measured incident directions are sorted into a spherical Delaunay triangle mesh (Figure 5), then a Lagrangian mass transport plan is calculated along each Delaunay edge. This defines how one radial basis system transports into its neighboring radial basis system between vertices in the Delaunay mesh such that the energy used to move the first distribution to the second distribution is minimized. This "cost" function is based on Earth Mover's Distance (EMD). The transport plan is encoded in a coefficient matrix, where the number of rows corresponds to the source Gaussian lobes and the number of columns to the destination Gaussian lobes. Each coefficient in this sparse matrix indicates the amount of energy from one lobe that is conveyed to another lobe. This enables one to create any radial basis system along the edge by partial displacement as described in [Bonneel et al. 2011]. The method has been extended to include points in the interior of each incident direction triangle by interpolating first across one edge then towards the opposite vertex. The result is an outgoing scattering interpolant representation (SIR) for each measured incident angle. The SIR file contains the Gaussian lobe parameters corresponding to each RBS and a

transport plan (coefficient matrix) representing each edge in the Delaunay mesh. There is one SIR file per incoming/outgoing hemisphere pair, so up to four SIR files for a single material.
Step 4: BSDF symmetry is deduced based on measured incident directions: isotropic (90° arc), quadrilateral (quarter hemisphere), bilateral (half hemisphere), or anisotropic (no symmetry, full hemisphere); e.g., an RBS derived for an isotropic material is used for all other φ angles in the same θ band. Symmetry and Lagrangian interpolation are applied to complete the four-dimensional BSDF by interpolating two or three vertices in the Delaunay mesh.

Step 5: The SIR is then used to interpolate the BSDF to a more convenient representation (Klems matrix or tensor tree basis) for use in simulations of annual performance (Figure 6). Where greater accuracy or angular resolution is needed, the tensor tree basis is used, which subdivides as needed around peaks in the distribution for more time- and space-efficient simulations. For the Klems basis (using *bsdf2klems*), the SIR is evaluated at each of the 145 angles of incidence (from a central position within the Klems patch), where 250 or so samples is sent to each exiting patch in the Klems matrix to get a good average result. In all, it takes about 21 million samples (four hemispheres, 145×145 basis, 256 samples), which is a few minutes on a single processor. For the tensor tree basis (using *bsdf2ttree*), interpolation must be done for many more incident patches corresponding to the maximum tensor tree resolution being targeted. For the default tensor tree (–t3 6, where k=6 refers to generation of $2^{2\cdot6}$ directions per hemisphere), there are 4096x4096 directions per hemisphere pair, which is 28 times as many as the Klems basis. Each scattered direction gets a single sample. It can take over an hour to interpolate a tensor tree from an SIR file. Before the tree is saved, it is reduced (pruned) by *rttree_reduce*, a separate tool that is called by *bsdf2ttree* (and *genBSDF*) to prune similar branches and simplify the tree to reduce subsequent storage and computation costs. An example tensor tree with adaptive resolution is shown in Figure 2, and plotted in 3-D in Figure 6.

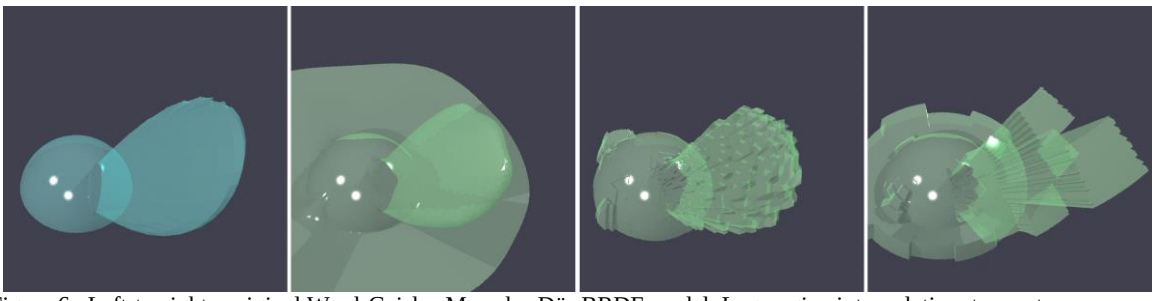

Figure 6. Left-to-right: original Ward-Geisler-Moroder-Dür BRDF model, Lagrangian interpolation, tensor tree representation, Klems representation.

Step 6: The complete BSDF data can be used for simulations of annual performance using the three- or five-phase methods. As is the case with the synthetic BSDFs, the diffuse sky (scattering) component of the five-phase method can be computed using the Klems BSDF data derived from the SIR file while the direct sun component can be computed using the geometry of the system (e.g., venetian blind geometry) or the tensor tree BSDF data derived from the SIR file.

4. Validation

4.1. Validation of the interpolation tool using a synthetic BRDF model

A validation of the interpolation tool was conducted comparing interpolated data to simulated "measurement" data. This data set was generated using a mathematical BRDF model (Ward-Geisler-Moroder-Dür model [Geisler-Moroder and Dür, 2010]) that was sampled at locations typical of the LBNL scanning goniophotometer, shown in Figure 7. A total of 88 incident directions and 225,000 measurement

locations were used to generate the simulated BRDF measured data set (Figure 7). An uncorrelated set of 12,300 incident and outgoing test directions were generated using the interpolation tool from this virtually measured data set. The root mean square (RMS) difference between the analytical BRDF model (i.e., ground truth) and the interpolated results was computed for the 150,000,000 incident and exiting test direction pairs (12,300 squared). RMS errors are listed in Table 2 for the interpolation alone, the converted tensor tree representation at 16Kx16K resolution, and the Klems representation. An example of one incident direction is shown in Figure 6. (The BRDF spread at the horizon in the second image is due to a 1/cosine factor that does not affect the results.) The RMS difference between the interpolated data and the tensor tree and Klems representations are given in the last two rows of the table. These are the errors one might expect from these representations if interpolation were not necessary (i.e., if one had complete and noiseless measurements).

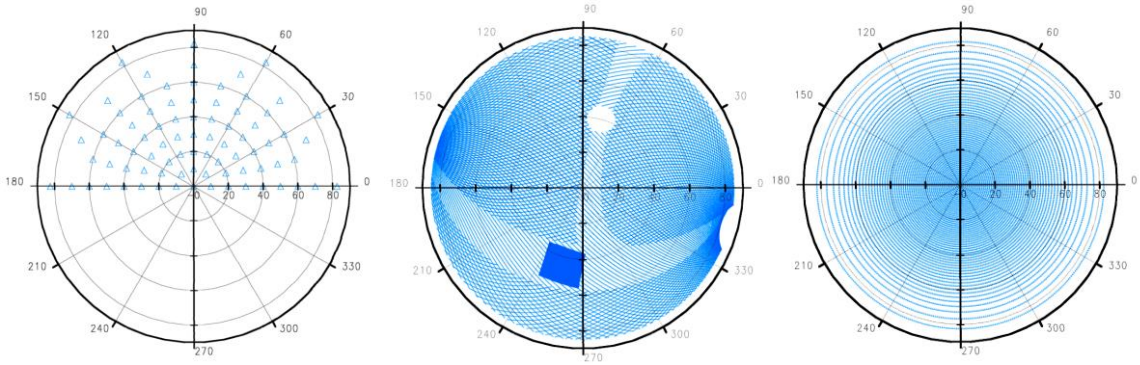

Figure 7. Left: The 88 incident sampling directions used in the simulated BRDF measurements. Center: The 225,000 BRDF sampling directions for a single incident direction at $(\theta,\phi) = (40°,75°)$. The dark patch is the concentrated sampling pattern in the expected specular (mirror) direction. Right: The 12,300 directions used for testing the interpolation (both incident and outgoing).

Table 2. RMS errors associated with interpolant and BRDF representations for all angles and for a subset of data that excludes incident and reflected angles > 75° from normal.

Reference	Compared to	RMS Difference	
		All data	Data for angles <75°
BRDF model	Interpolant	0.243	0.114
BRDF model	Tensor tree	0.282	0.138
BRDF model	Klems matrix	0.352	0.215
Interpolant	Tensor tree	0.139	0.076
Interpolant	Klems matrix	0.198	0.156

The RMS errors are larger than one might expect, and careful study shows that these errors mostly occur for incident angles greater than 75° from the surface normal. If these sample points are excluded, errors are reduced considerably. Note that the RMS errors are larger with the Klems representation (as one might expect from looking at the plots in Figure 6). This also demonstrates that the RMS error of the interpolant roughly doubles when incident angles greater than 75° from normal are included – these interpolation errors go on to dominate the other sources of error in the BSDF representation. Since transmission through window glazing is low for grazing angles beyond 75° and is often blocked by nearby opaque façade elements (e.g., window frame), interpolation errors in this region may be less important.

It is often more informative to study the error population of an interpolation method. Figure 8 shows the percentile of resampled positions that achieve a given absolute error relative to the BRDF reference model for the straight interpolant, the tensor tree and the Klems representations. Evident in this plot is that the interpolant itself achieves better than 4% error for 90% of BRDF samples less than 75° from normal. Including the tensor tree, this relative error increases slightly to 6% for 90% of values, which is also roughly met by the Klems representation. However, significantly more of the Klems values have large relative errors due to the coarse resolution of 145 incident and reflected angles, as shown in the asymptotes of the three curves. The slower rise of the tensor tree curve is a side-effect of using relative error, which makes smaller BRDF values contribute more. In this case, the smaller values are the constant portion of the test BRDF model, where the Klems representation works well exactly because it has poor resolving power.

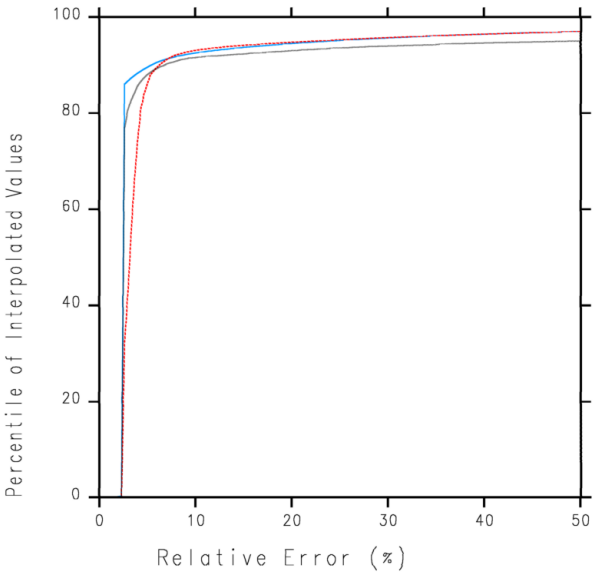

Figure 8. Error population for the scattering interpolant representation (SIR, blue line), and the tensor tree (red line) and Klems (gray line) representations relative to the BRDF reference model.

A key question to consider when optimizing the BSDF measurement procedure is how many incident directions are needed to obtain a reasonably accurate interpolated result. Table 3 shows the effect of decreasing the number of measured incident directions using the same BRDF model described in the previous section. The three-dimensional plots in the fourth row compare the reference distribution (light blue) to the interpolated result using the given incident directions. Notice how 32 incident directions capture the synthetic BRDF nearly as well as 88 measurements in this example. Even 13 incident angles produces a reasonable result, although the peak is somewhat displaced from its original location. With seven incident directions however, the interpolation has lost its shape completely. From this small number of tests, it appears that somewhere between 30 and 40 incident angles should be sufficient per half-hemisphere, although we expect this will depend somewhat on the material's behavior [Grobe et al. 2017b]. For surfaces with quadrilateral symmetry, the number of incident directions can probably be reduced to between 17 and 25 angles (being sure to capture the azimuthal borders). For completely asymmetric samples with irregular or complex distributions, 50-75 incident measurements may be sufficient.

Table 3. Comparison of RMS error given incident sampling direction densities.

No. of Angles	88	32	13	7
RMS Error (<75°)	0.114	0.117	0.142	0.744
Incident Directions	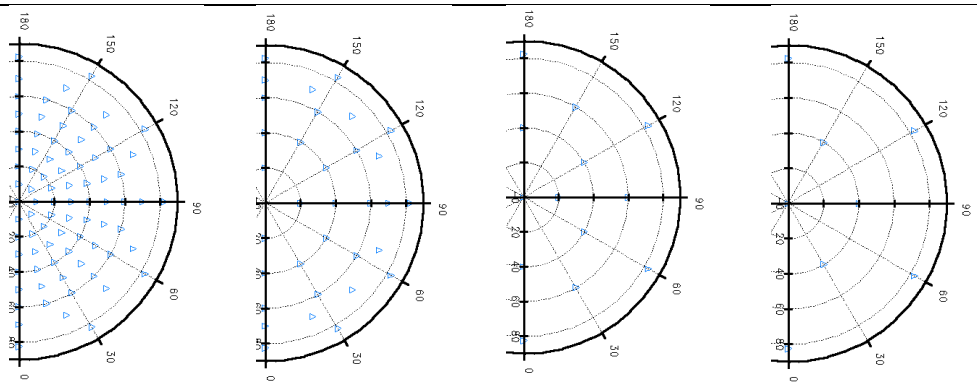			
3-D Plot	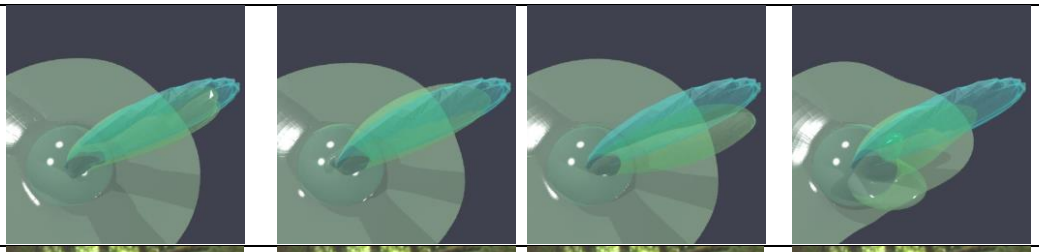			
Rendering	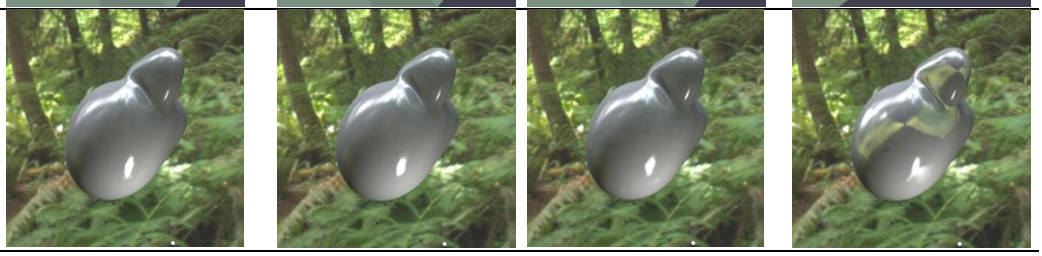			

4.2. Field validation of the five-phase method

For the validation of the five-phase method (Equations 4-5), a total of four different window configurations were measured in the field. Two daylighting films and an exterior micro-louvered solar screen were evaluated sequentially in a full-scale FLEXLAB testbed located at the Lawrence Berkeley National Laboratory in Berkeley, California [Lee et al. 2016]. A reference room with a conventional venetian blind was monitored simultaneously in an adjacent identical test cell. The systems were installed in the south-facing window of a 6.1 m wide by 9.1 m deep by 2.7 m high (20x30x9 ft) conditioned space fitted with low-height furniture and recessed LED lighting to emulate a typical open plan office (Figure 9). Global and diffuse horizontal solar irradiance (Delta-T Devices, SPN-1, ±8% of reading in 0-2000 W/m^2 range) measured on the roof of the testbed facility were sampled and recorded 1/s with the mean recorded at a 1-min interval. Daylight illuminance was measured similarly at workplane height with a two by five grid of illuminance sensors (LiCor LI-210SA, ±3% of reading, 0-5000 lux range near the window, 0-2000 lux range further from the window). Field-of-view luminance data were collected every 5 minutes using an automated system that captured low dynamic range (LDR) images with a Canon EOS 5D digital camera and Sigma 4.5 mm/ f2.8 circular fisheye lens, then composited the LDR images into a single high dynamic

range (HDR) image (using Radiance *hdrgen*). The image was calibrated so that the calculated vertical illuminance derived from the HDR image matched that of the vertical sensor positioned immediately adjacent to the fisheye lens. Fisheye projection and vignetting corrections were applied to the LDR images prior to conversion to the HDR image. The HDR images (799x799 pixels[6]) were analyzed using the default settings in the *evalglare* software [Wienold 2016, Wienold and Christoffersen 2006] to compute the daylight glare probability (DGP) and daylight glare index (DGI) from each of the captured viewpoints within the room.

Figure 9. Photograph of the interior of the FLEXLAB testbed office with an exterior roller shade partially lowered over the south-facing window.

Two daylight-redirecting films were evaluated sequentially (DL-L1 (Lucent Optics) and DL-L2 (Serraglaze)), both with microscopic features designed to redirect sunlight for a specified range of profile angles[7] (i.e., 42-65°) and transmit sunlight specularly for angles outside this range. Each film was mounted inboard of the dual-pane low-emittance glass in the upper third of the window with the lower two-thirds of the window covered by a 2.54-cm wide, matte white, indoor venetian blind set to a fixed cut-off angle of 20°. An exterior shading system was also evaluated (S-L (SmartLouver)). This solar screen consisted of matte black, horizontal flat slats that were 1.25-mm wide and 0.22-mm thick with a fixed cut-off angle of 40°. The screen was installed to cover the entire exterior surface of the window. In the adjacent reference room, an indoor venetian blind (ref-VB) was installed to cover the entire window. The blind type and slat angle were the same as that used in the test room.

[6] This default recommended image size results in reasonable runtimes for industry. The 799×799 image size has about 501,000 pixels in a 180º fisheye image. The sun orb would be represented by an average of 4.8 pixels in the HDR image (greater resolution than the five-phase method's simulated image).

[7] The profile angle is the angle of the sun projected onto the vertical plane perpendicular to the facade. It is used in the context of linear systems, for example, as their behavior can be characterized simply with profile angle (e.g., cut-off profile angle).

The BSDF for the conventional venetian blind was generated using the *genBSDF* ray-tracing tool given the geometry and reflectance of the slat material. For the direct sun component of the five-phase method, the geometry of the venetian blind was used. The three remaining fenestration systems were measured using the LBNL scanning goniophotometer with angles of incidence at 15° increments of φ and 10° increments of θ, assuming left-right hand symmetry (81 total angles of incidence). Detailed scans were made in areas of peak transmission. The measured data were then interpolated using *pabopto2bsdf* to create a radial basis system interpolant which was then used by the *bsdf2klems* and *bsdf2ttree* utilities to produce the final BSDF XML files in the Klems and tensor tree format. The tensor tree basis was resolved to a resolution equal to apex angles as small as 1.5° (option –t4 7, 6.4 times the solid angle of the sun) for all three fenestration systems.

Workplane and vertical illuminance, field-of-view luminance, and discomfort glare data were generated using the three- and five-phase (from Equation 5) methods to compare against the measured data. The Perez sky model was used to produce the **S** matrix, using the monitored 5-min solar radiation data from the site and the Tregenza basis subdivided by a factor of 16 (Reinhart MF:4). Monitored 5-min illuminance and luminance data from one week during the equinox period for each of the modeled systems were used for the comparisons.

Results from the comparison are given in Table 4, where the frequency of deviation (expressed as the percentage of the monitored period) of the simulated results from measured data is given for each of the four fenestration systems. The ideal would be a modeling approach that achieves less than 5% deviation from measured results for 100% of the monitored period. The 5% deviation is the estimated level of measurement error of solar conditions, positional error with indoor sensors, and inaccuracies in representing the real world conditions of the room interior and outdoor conditions. For the DL-L1 system, for example, workplane illuminance computed using the three-phase method deviated from measured results by less than 5% for only 16.8% of the monitored period, while the five-phase method was able to achieve less than 5% deviation for 29% of the monitored period. DGI proved to be the most difficult to match. This metric relies on accurate modeling of both the spatial distribution and intensity of glare sources within the field of view so small shifts in view angle can result in significant errors between predicted and measured results. DGP is strongly correlated to vertical illuminance at the eye and is therefore less dependent on spatial accuracy of glare sources. For this metric and for vertical illuminance, the modeled data matched measured results more closely.

The frequency of deviation for all four fenestration systems for deviations less than 10% is plotted in Figures 10 and 11 to more easily visualize the results for the three- and five-phase methods. In Figure 10, points above the diagonal line indicate the higher percentage of the monitored period when the five-phase method had a deviation of less than 10% compared to the three-phase method. For horizontal and vertical illuminance, the five-phase method deviated from measured data less frequently than the three-phase method by about 20-40% of the monitored period. In Figure 11, points below the diagonal line indicate the higher percentage of the monitored period when the three-phase results deviated from measured data by 20% or more compared to the five-phase method.

Table 4. Frequency of deviation (percentage of the equinox monitored period) when the difference between the simulated and measured data was less than 5%, 10%, or 20% or was equal to or greater than 20%.

Ehoriz	five-phase				three-phase			
	$\Delta < 5\%$	$\Delta < 10\%$	$\Delta < 20\%$	$\Delta \geq 20\%$	$\Delta < 5\%$	$\Delta < 10\%$	$\Delta < 20\%$	$\Delta \geq 20\%$
DL-L1	29.0%	53.9%	85.0%	15.0%	16.8%	33.5%	58.3%	41.7%
DL-L2	28.2%	61.3%	92.9%	7.1%	26.7%	55.2%	86.9%	13.1%
S-L	25.0%	50.9%	74.1%	25.9%	28.2%	55.1%	78.7%	21.3%
Ref VB	31.9%	73.0%	94.3%	5.7%	15.7%	42.7%	94.9%	5.1%
Ref VB	44.5%	85.7%	94.5%	5.5%	17.9%	46.9%	95.1%	4.9%
Ref VB	35.2%	70.2%	88.3%	11.7%	22.7%	49.4%	88.1%	11.9%

Evert	five-phase				three-phase			
	$\Delta < 5\%$	$\Delta < 10\%$	$\Delta < 20\%$	$\Delta \geq 20\%$	$\Delta < 5\%$	$\Delta < 10\%$	$\Delta < 20\%$	$\Delta \geq 20\%$
DL-L1	20.6%	52.1%	92.0%	8.0%	16.3%	35.6%	75.9%	24.1%
DL-L2	33.1%	75.5%	96.3%	3.7%	18.2%	47.0%	89.4%	10.6%
S-L	21.9%	41.0%	65.1%	34.9%	22.7%	45.2%	67.7%	32.3%
Ref VB	40.0%	74.0%	87.5%	12.5%	14.8%	30.8%	81.2%	18.8%
Ref VB	49.8%	77.9%	90.9%	9.1%	22.0%	45.5%	89.7%	10.3%
Ref VB	23.6%	54.9%	75.8%	24.2%	14.2%	29.5%	72.8%	27.2%

DGP	five-phase				three-phase			
	$\Delta < 5\%$	$\Delta < 10\%$	$\Delta < 20\%$	$\Delta \geq 20\%$	$\Delta < 5\%$	$\Delta < 10\%$	$\Delta < 20\%$	$\Delta \geq 20\%$
DL-L1	36.6%	74.5%	99.7%	0.3%	16.7%	32.7%	84.4%	15.6%
DL-L2	62.7%	94.8%	99.4%	0.6%	23.9%	75.9%	94.2%	5.8%
S-L	82.4%	93.1%	98.1%	1.9%	83.8%	93.1%	97.7%	2.3%
Ref VB	76.5%	97.5%	100.0%	0.0%	39.2%	91.7%	97.1%	2.9%
Ref VB	76.7%	100.0%	100.0%	0.0%	60.2%	99.2%	100.0%	0.0%
Ref VB	68.0%	81.8%	97.6%	2.4%	29.8%	80.6%	90.6%	9.4%

DGI	five-phase				three-phase			
	$\Delta < 5\%$	$\Delta < 10\%$	$\Delta < 20\%$	$\Delta \geq 20\%$	$\Delta < 5\%$	$\Delta < 10\%$	$\Delta < 20\%$	$\Delta \geq 20\%$
DL-L1	14.7%	28.7%	48.5%	51.5%	3.9%	6.6%	11.3%	88.7%
DL-L2	8.6%	16.5%	53.9%	46.1%	4.1%	10.3%	18.3%	81.7%
S-L	36.1%	56.6%	78.2%	21.8%	37.7%	56.5%	78.2%	21.8%
Ref VB	14.8%	25.2%	68.7%	31.3%	16.5%	30.9%	56.2%	43.8%
Ref VB	15.9%	32.6%	72.4%	27.6%	21.3%	41.8%	75.8%	24.2%
Ref VB	16.5%	36.3%	64.6%	35.4%	9.2%	15.7%	33.9%	66.1%

Notes: Ehoriz = horizontal illuminance at 1.8 m from the window, Evert = vertical illuminance facing west at 1.8 m from the window and 1.2 m above the floor, discomfort glare DGP and DGI facing west at same location as Evert.

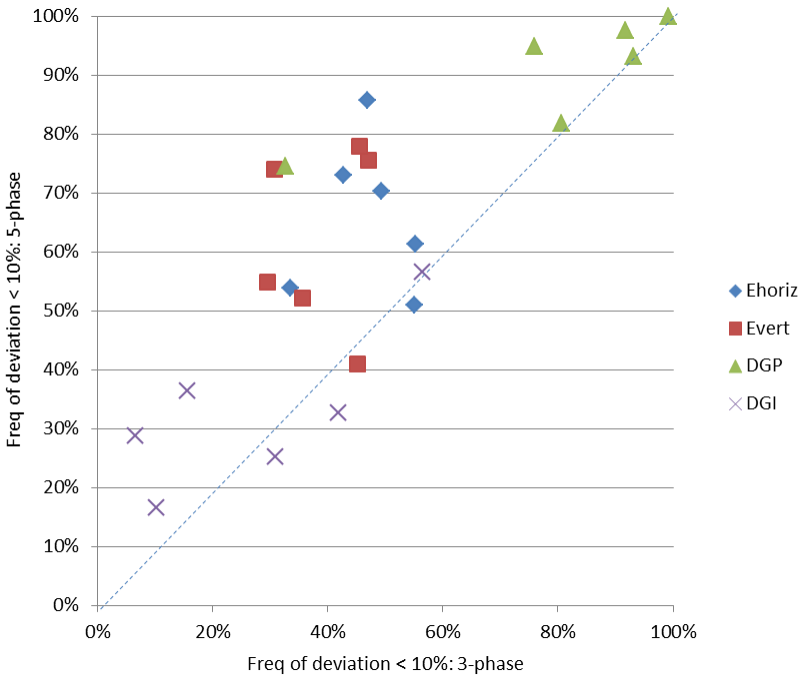

Figure 10. Frequency of deviation (percentage of the equinox monitored period) when the difference between the simulated and measured data was less than 10%, where the simulated data were determined using the three-phase (x-axis) or the five-phase (y-axis) method. Each point represents one week of monitored data for one type of fenestration system.

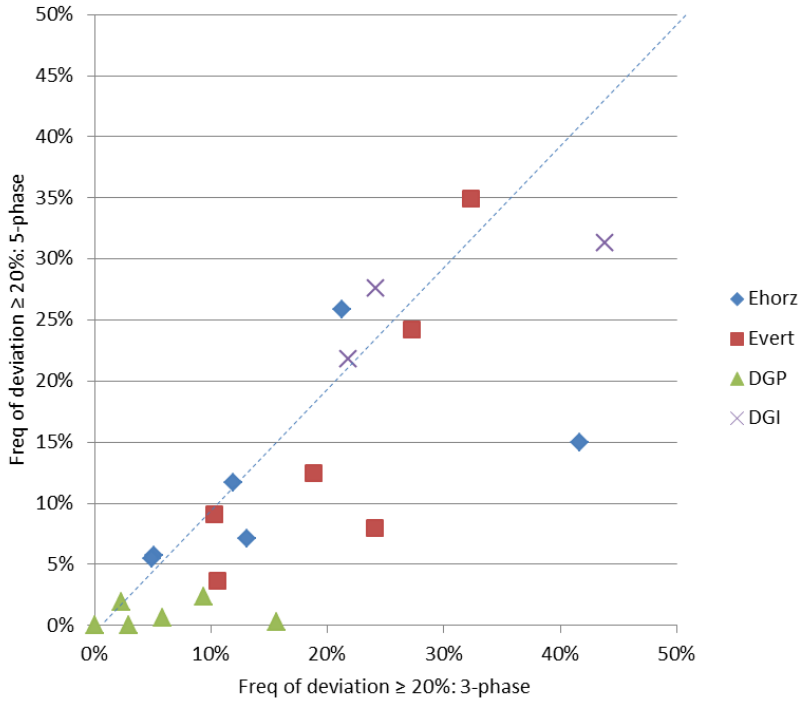

Figure 11. Frequency of deviation (percentage of the equinox monitored period) when the difference between the simulated and measured data was equal to or greater than 20%, where the simulated data were determined using the three-phase (x-axis) or the five-phase (y-axis) method.

Overall, the five-phase method resulted in closer agreement with the measured data for a larger percentage of the equinox monitored period than the three-phase method. Spatial and temporal differences in predicted values from measured data were in part due to the resolution of BSDF input data and the various matrices.

Other errors were caused by differences between actual and modeled sun and sky conditions, simplifications in the office model, and slight positional differences with sensors relative to the fenestration system. Note also that when daylight levels were low, small absolute differences between predicted and measured data resulted in large percentage errors.

Analysis during the equinox period had fewer hours when direct sun was present in the room. A similar analysis was conducted for the winter solstice period to more extensively test the accuracy of the five-phase method when low angle sunlight entered the space. Comparisons with the DL-L1 and DL-L2 systems, however, indicated that results under sunny conditions were confounded by inaccurate modeling of the lower venetian blinds, whose actual slat angles varied over the height of the blind and between each of the three adjacent blinds. Comparisons with the S-L exterior micro-louvered screen revealed similar issues. Results from the three- and five-phase methods diverged significantly from measured results, potentially because of small spatial inaccuracies between the angle of the sun relative to the micro-louvers or inadequate characterization with the measured BSDF data set (e.g., potential variation in actual micro-louver angle at the testbed compared to the small sample measured with the scanning goniophotometer). An example of the S-L comparison is shown in Figure 12. The measured data show periods (9:30-10:30 AM, 1:45-2:15 PM) when sunlight is detected by the sensor (sensor tops out at 5500 lux) and when the sensor is shaded by the window frame (between 11:30-12:30). Both the three- and five-phase methods show only a modest increase in workplane illuminance when the desk is sunlit (3500 lux maximum) versus shaded (1000 lux).

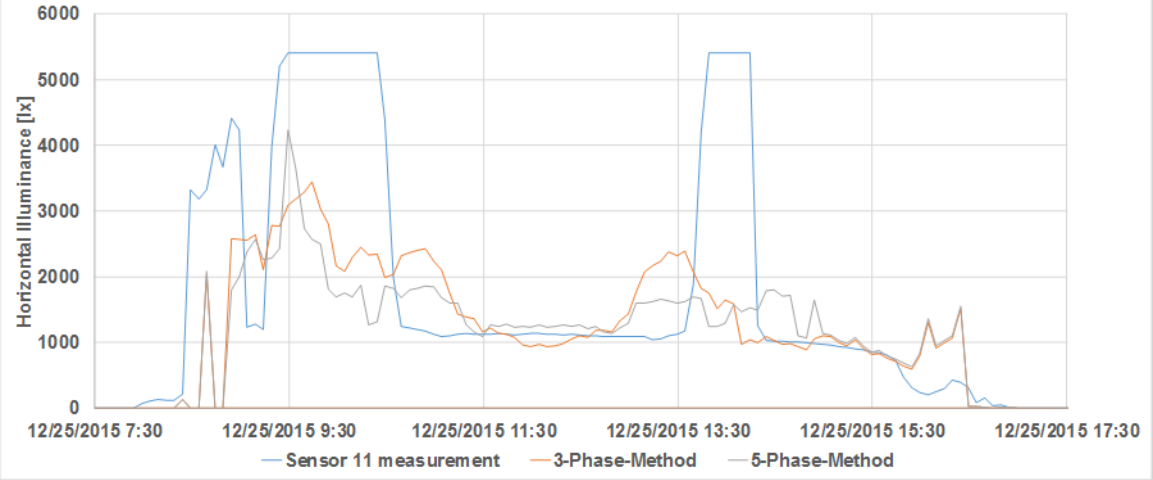

Figure 12. Measured and modeled workplane illuminance (lux) in the south-facing testbed office on a sunny winter day, December 25.

4.3. Validation against ray-tracing simulations

The discrepancies between measured and simulated data in Section 4.2 included all errors associated with sample irregularities, BSDF measurements, interpolation, modeling approach, physical conditions of the

field test site and installation, and limits of the sensors and data acquisition system in a real-world environment. In order to estimate the error due solely to the five-phase method, without the additional inaccuracies introduced by BSDF measurements and the interpolation tool, a second comparison was made by modeling a simple clear glass layer with the three- and five-phase methods and comparing the results to "ground truth" simulations using the validated (e.g., [Geisler-Moroder and Dür 2008]) Radiance ray-tracing tools *rtrace* and *rpict*.

The three modeling approaches used the same geometric model of the full-scale test room. Total and diffuse horizontal irradiances from the monitored study for the winter period were fed into Radiance tools *gendaylit* and *gendaymtx* to generate Perez sky descriptions for the ground truth renderings and the phase methods, respectively. The BSDF data sets for the clear glazing were generated with *genBSDF* in the Klems and variable resolution, tensor tree (–t3 6) formats. The ground truth simulations were performed with the geometry of the glazing modeled by a glass *material*. The three-phase method simulations used the Klems representation of the glass model. The five-phase method used geometry or a high resolution BSDF for the calculation of the direct sun component.

Discrepancies between the three-phase method and the monitored results in Section 4.2 were due in part to local patterns of sunlight and shadow (Figure 13). For the clear glass, this is particularly evident in the rendered images (Figure 14) as well as in the time-of-day plots of horizontal illuminance (Figures 15-16). Note the absence of a shadow line from the window framing system in the three-phase method's rendering. Small geometric effects were not reproduced because the Klems low-resolution basis spread the sun's luminous flux over a large solid angle, resulting in blurred illuminance distributions. This can also be seen in the horizontal illuminance data for sensor #2, when the sensor is shaded by the horizontal frame between the upper and lower window sections around noon for several hours (Figure 16). This effect cannot be seen in the results generated by the three-phase method.

In the assessment of discomfort glare, small modeling details can produce significant differences in the resultant image and discomfort glare rating. For example, the *gendaylit* model for the *rpict* dataset produces a sky with a continuous luminance distribution, as seen in the rendered image. With *gendaymtx*, the five-phase method uses the Tregenza/ Reinhart MF:4 subdivision for the sky component and MF:6 subdivision for the sun component. Since the renderings were generated on a 5 min timestep, the sun position was off by about 1.5° between the *rpict* and five-phase method renderings (note how the shadow line of the window mullion is at slightly different angles in Figure 14). The images were also rendered with a resolution of 512x512 pixels (to reduce computation time) for the DGI and DGP calculations. In some cases, the orb of the sun was rendered with two pixels and in other cases, with four pixels resulting in significant differences in the rendered intensity of the sun (this occurred for both the *rpict* ray-tracing and matrix methods). Again, for metrics that rely on accurate spatial and intensity modeling of luminance like DGI, these small details can result in significant discrepancies between the ground truth and the five-phase method.

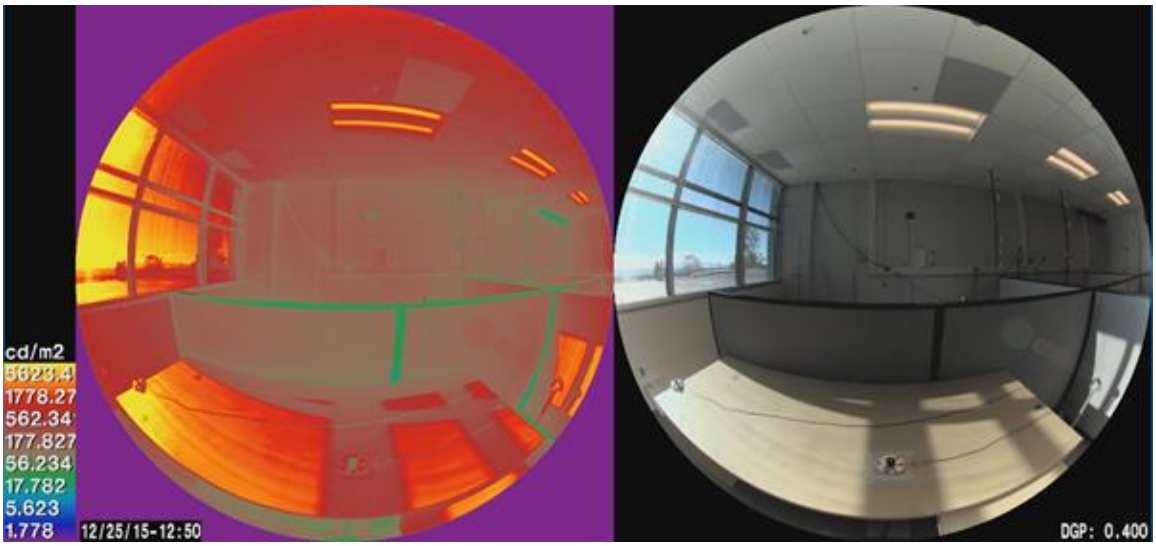

Figure 13. HDR image (left) and photograph (right) of the full-scale testbed with the S-L exterior screen system showing the shadow pattern on the workplane illuminance sensor #2 in the foreground while sensor #1 to the left is in direct sunlight, December 25, 12:50 PM.

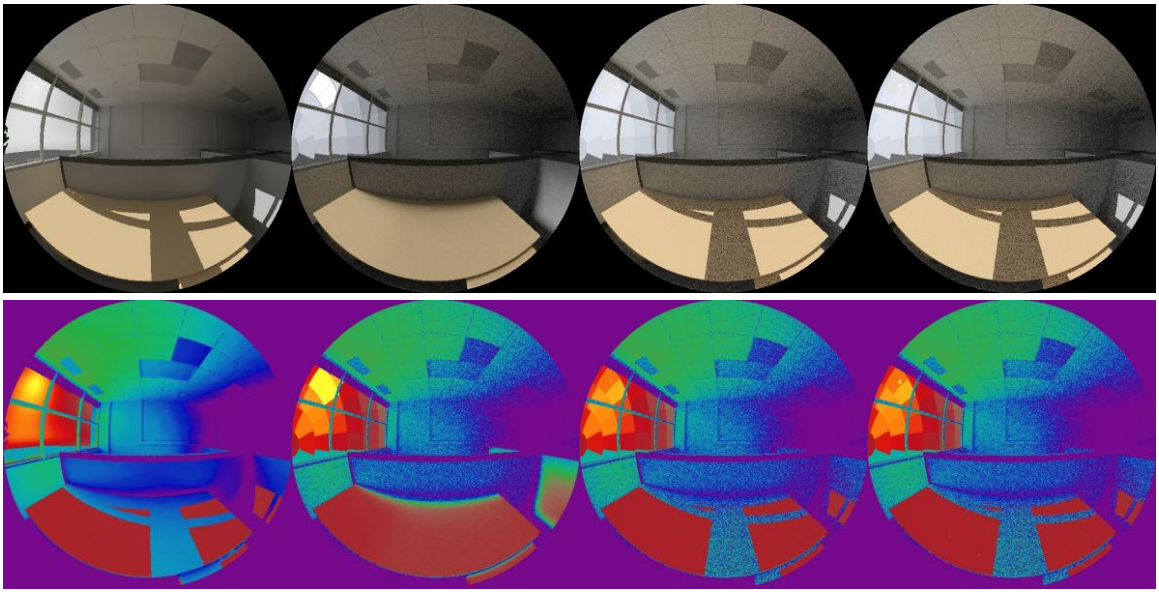

rpict rendering ("ground truth")

three-phase method

five-phase method (system via geometry)

five-phase method (system via BSDF –t3 6)

Figure 14. Photorealistic views (upper row) and falsecolor luminance images (lower row) of the room interior with clear glass windows rendered using different modeling approaches, December 25, 12:50 PM. All luminance images have the same falsecolor scale.

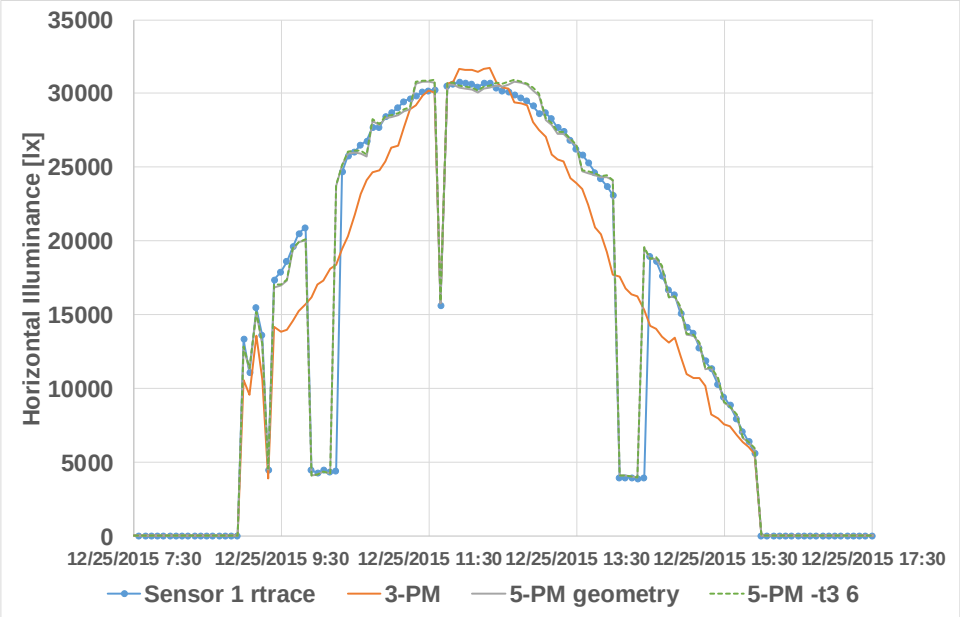

Figure 15. Clear glass. Horizontal illuminance at sensor #1 (0.9 m from the window) modeled using four different modeling approaches, with *rtrace* as the ground truth, December 25.

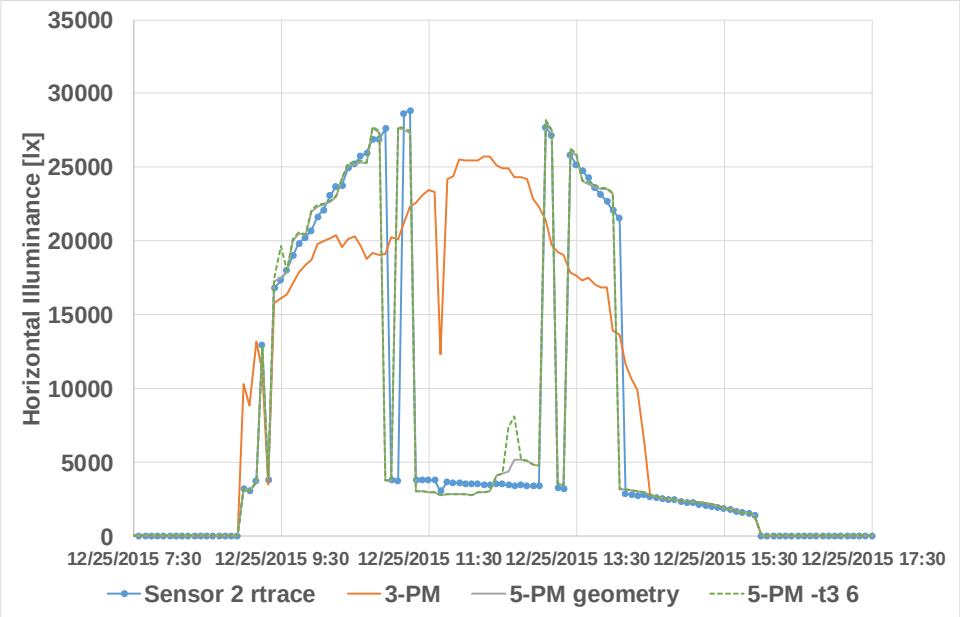

Figure 16. Clear glass. Horizontal illuminance at sensor #2 (1.8 m from the window) modeled using four different modeling approaches, with *rtrace* as the ground truth, December 25.

Despite these discrepancies, the frequency of deviation for the various modeling approaches shows that the five-phase method clearly outperforms the three-phase method in scenes with direct sunlight penetration (Table 5 and Figure 17). The five-phase method is able to match the ground truth horizontal illuminance sensor #1 (Ehoriz1) to within 5% for 91% of the modeled period compared to 40% of the period with the three-phase method. For sensor #2 shaded on occasion by the window frame, the five-phase method matched ground truth within 20% for 88% of the period compared to 47% of the period with the three-phase method.

Concerning discomfort glare evaluations, DGP results were comparable to that of vertical illuminance (Figure 18), given that vertical illuminance is the primary driver in the DGP formula. With the daylight glare index (DGI), which strongly depends on the position and luminance of glare sources within the field of view, the five-phase method shows a marked improvement over the three-phase method.

Table 5. Clear glass. Frequency of deviation (percentage of winter monitored period) when the difference between the gold standard ray-traced data and three- or five-phase methods' generated data was less than 5%, 10%, or 20% or was equal to or greater than 20%.

	three-phase method				five-phase method				
	Δ<5%	Δ<10%	Δ<20%	Δ≥20%	C_{ds}	Δ<5%	Δ<10%	Δ<20%	Δ≥20%
Ehoriz1	40%	53%	72%	28%	geometry	91%	96%	96%	4%
					BSDF –t3 6	91%	96%	96%	4%
Ehoriz2	21%	38%	47%	53%	geometry	60%	81%	88%	12%
					BSDF –t3 6	58%	78%	87%	13%
Evert	43%	62%	80%	20%	geometry	72%	91%	97%	3%
					BSDF –t3 6	69%	90%	97%	3%
DGP	60%	65%	73%	27%	geometry	77%	89%	93%	7%
					BSDF –t3 6	68%	77%	88%	12%
DGI	4%	9%	22%	78%	geometry	49%	69%	81%	19%
					BSDF –t3 6	12%	55%	76%	24%

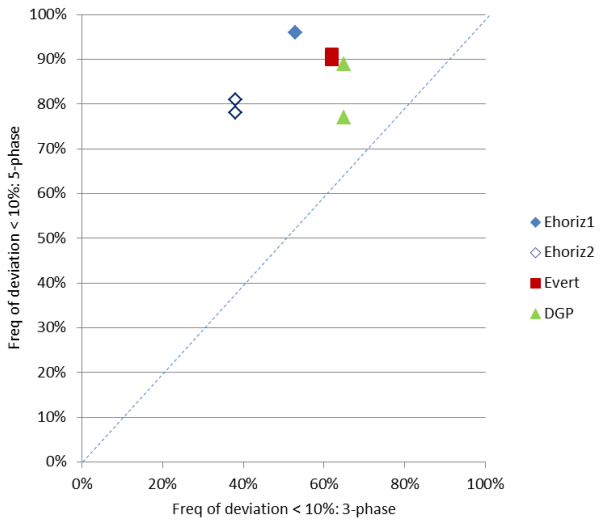

Figure 17. Clear glass. Frequency of deviation (percentage of winter monitored period) when the difference between data generating using the matrix methods versus *rtrace* ray-tracing method was less than 10%. Frequency of deviation for the three-phase method is shown on the x-axis and for the five-phase method on the y-axis.

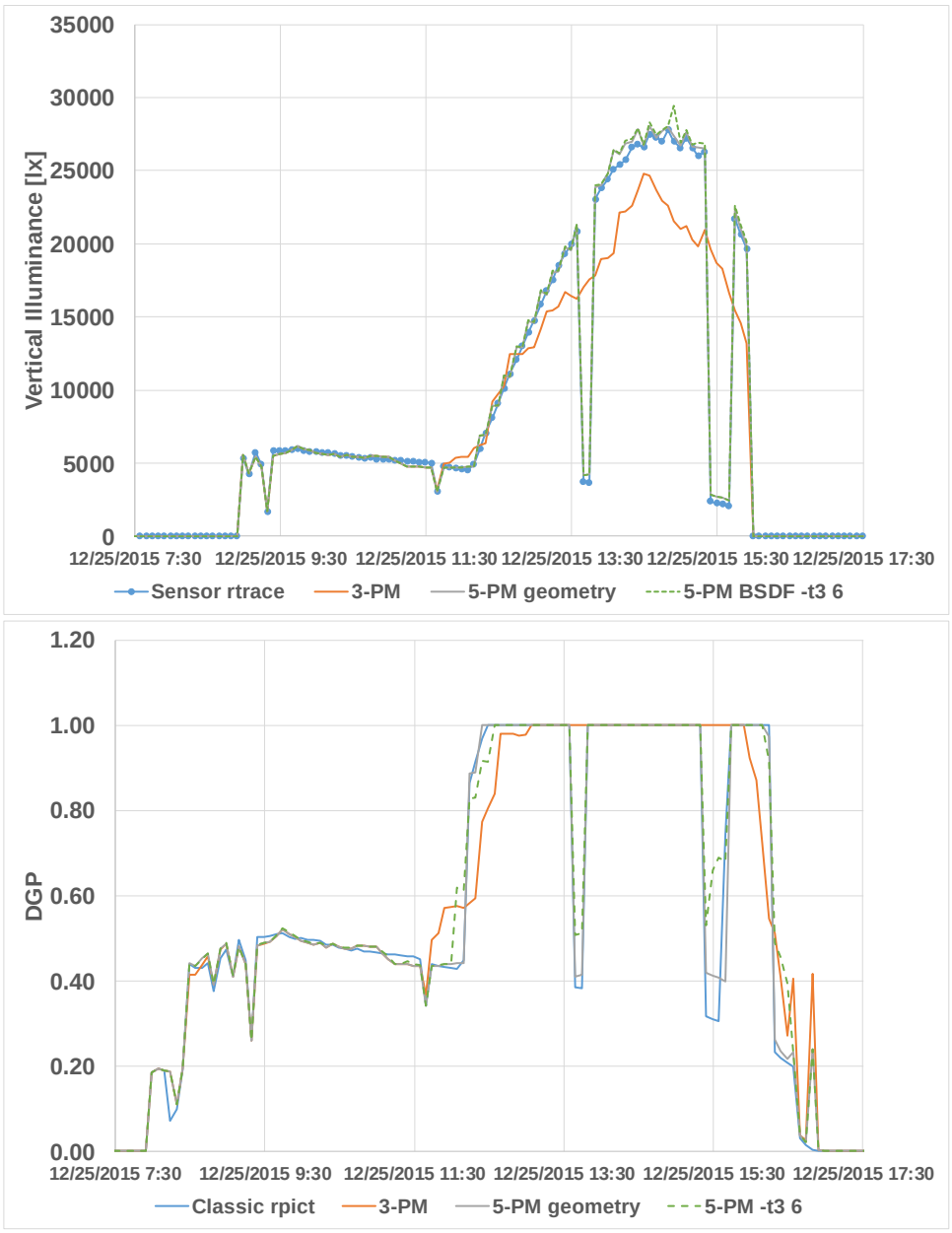

Figure 18. Clear glass. Comparison of vertical illuminances at the eye for a typical user position (upper) and DGP values as experienced at this point (lower) on December 25.

5. Conclusions

As stated in the introduction, many open source and proprietary modeling tools have incorporated the three-phase modeling approach to compute both window heat gains and daylighting performance. These software tools have and are being used on real world design projects to assess compliance with green building standards, to develop new energy-efficiency or other daylight metric standards, to develop and assess emerging technologies, and to rate and certify commercially-available shading and daylighting products. BSDF datasets developed for common shading systems have become available as organizations such as LBNL develop and publish libraries that can be openly accessed by industry.

This study does not define which of the three- or five-phase methods is suitable for specific applications. Results from this validation only indicate that the five-phase method delivers superior accuracy compared to the three-phase method: agreement with measured data was to within 20% for greater than 75% of the monitored period for illuminance-based performance parameters (horizontal and vertical illuminance, DGP). If the end user desires greater accuracy with respect to "ground truth" and the computational speed of a matrix operation for annual performance evaluations, particularly if operable fenestration systems are involved, then the five-phase method should be used.

This outcome precipitates the need for several actions on the part of industry. To avoid inadvertent use of BSDF input data with insufficient accuracy, libraries should stipulate either how the BSDF data were derived or how the specular component was characterized. The current LBNL BSDF library, for example, was developed for the purpose of evaluating solar heat gain, not daylighting or visual discomfort. Similarly, software tools should stipulate which modeling algorithms are being used so that the end user can make more informed decisions. EnergyPlus implements the three-phase method for solar heat gain calculations, for example, but retains the old split-flux method for daylighting.

Measurement protocols will need to be developed to more accurately characterize specular transmission and reflectance properties of fenestration materials and systems. Measurement equipment will also need to meet certain specifications with respect to angular resolution and dynamic range. There is a considerable amount of work that has to be conducted to develop practical methods for characterizing the thousands of shading and daylighting materials and systems currently available on the market. For systems that can be characterized using ray-tracing tools and simple measurements of the base material, some degree of quality control should be exerted if BSDF data sets are to be shared between end users or across the open source community.

Software developers are beginning to incorporate the five-phase method into existing software tools [Roudsari 2017]. The five-phase method requires significantly more pre-processing time to generate the necessary matrices, particularly for discomfort glare analysis, and can take longer to perform the actual matrix operations for annual simulations.

While the five-phase method is superior to the three-phase method, this validation study made evident that the five-phase method is reliant on a precise calculation of the unscattered transmitted direct sun component. In the course of this study, an initial approach was implemented in Radiance that enables the calculation of the transmitted component through BSDFs for small light sources like the sun. A comprehensive implementation that relies on a concept of "peak extraction" may further lessen the possibility of over- and underestimation of the direct component. Specifically, methods for extracting and accounting of strong specular "through" and perhaps "mirror" directions will be needed. We could also investigate the possibility of representing specular peaks in other directions, though tracking these accurately over an entire BSDF is a research topic in itself.

Acknowledgments

This work was supported by the Assistant Secretary for Energy Efficiency and Renewable Energy, Building Technologies Program of the U.S. Department of Energy under Contract No. DE-AC02-05CH11231, by the California Energy Commission through its Electric Program Investment Charge (EPIC) Program on behalf of the citizens of California, by Pacific Gas and Electric Company's Emerging Technologies Program, and by the Austrian Research Promotion Agency (FFG) through the "lightSIMheat" project under Contract No. 838718. In-kind support was provided by Lucent Optics, Serralux, and SmartLouvre.

Amir Roth, U.S. Department of Energy, and Dustin Davis, California Energy Commission, provided invaluable support over the term of this research. We would also like to acknowledge the contributions of Wilfried Pohl and Christian Knoflach, Bartenbach GmbH, and LBNL team members Taoning Wang, Anothai Thanachareonkit, Jacob Jonsson, Christoph Gehbauer, Darryl Dickerhoff, Jordan Shackelford, Daniel Fuller, Ari Harding, Cynthia Regnier, and Stephen Selkowitz. Andrew McNeil and Christian Humann, Terrestrial Light, provided additional technical support related to the field validation.

References

AERC, Attachments Energy Rating Council, http://aercnet.org/, accessed June 5, 2017.

Andersen, M., Roecker, C., Scartezzini, J.-L., 2005a. Design of a time-efficient video goniophotometer combining bidirectional functions assessment for transmission and reflection, Solar Energy Materials and Solar Cells 88 (1): 97-118.

Andersen, M., Rubin, M., Powles, R., Scartezzini, J.-L., 2005b. Bi-directional transmission properties of Venetian blinds: experimental assessment compared to ray-tracing calculations. Solar Energy 78: 187-198.

Andersen, M., de Boer, J., 2006. Goniophotometry and assessment of bidirectional photometric properties of complex fenestration systems. Energy and Buildings 38: 836–848.

Andersen, M., Stokes, E., Gayeski, N., Browne, C., 2010. Using digital imaging to assess spectral solar-optical properties of complex fenestration materials: A new approach in video-goniophotometry. Solar Energy 84 (4): 549-562.

Apian-Bennewitz, P., von der Hardt, J., 1998. Enhancing and calibrating a goniophotometer. Solar Energy Materials and Solar Cells 54: 309-322.

Apian-Bennewitz, P., 2010. New scanning gonio-photometer for extended BRTF measurements. Proc. SPIE 7792, 77920O, Reflection, Scattering, and Diffraction from Surfaces II, September 1, 2010.

Arasteh, D.K., Selkowitz, S.E., Apte, J.S., LaFrance, M., 2006. "Zero Energy Windows." In 2006 ACEEE Summer Study on Energy Efficiency in Buildings. Pacific Grove, CA, 2006.

Aydinli, H., Kaase, H., 1999. Measurement of Luminous Characteristics of Daylighting Materials, Technical Report, International Energy Agency Solar Heating and Cooling Programme (IEA SHC) Task 21, 1999.

Bonneel, N., van de Panne, M., Paris, S., Heidrich, W., 2011. Displacement interpolation using Lagrangian mass transport, ACM Transactions on Graphics – Proceedings of ACM SIGGRAPH Asia 2011, Volume 30(6), Article 158:1-12.

de Boer, J., 2005. Modeling Indoor Illumination by CFS Based on Bidirectional Photometric Data; Technical Report, International Energy Agency Solar Heating and Cooling Programme (IEA SHC) Task 31, 2005.

de Boer, J., 2017. 2nd IEA SHC Task Definition Phase (TDF), “Integrated Solutions for Daylight and Electric Lighting”, Fraunhofer IBP, April 6-7, 2017, Copenhagen.

DOE, 2014. Windows and building envelope research and development: Roadmap for emerging technologies. U.S. Department of Energy, Energy Efficiency and Renewable Energy, Building Technologies Office, DOE/EE-0956, February 2014.

EnergyPlus 8.1, 2017. https://energyplus.net/, accessed June 8. 2017.

ES-SO, 2017. European Solar-Shading Organization, http://www.es-so.com/, accessed June 5, 2017.

Geisler-Moroder, D., Dür, A., 2008. Validation of Radiance against CIE171:2006 and Improved Adaptive Subdivision of Circular Light Sources. In 7th International RADIANCE Workshop (Fribourg, Switzerland, 2008).

Geisler-Moroder, D., Dür, A., 2010. A New Ward BRDF Model with Bounded Albedo, Computer Graphics Forum, Volume 29, Issue 4 (Proc. of EGSR 2010), pp. 1391-1398.

Geisler-Moroder, D., 2011. Validation of variable resolution BSDFs in Radiance. Bartenbach L-ichtLabor, November 2011, https://facades.lbl.gov/sites/all/files/varresbsdf-validation.pdf, accessed June 8, 2017.

Geisler-Moroder, D., Lee, E.S., Ward, G.J., 2017. Validation of the Five-Phase Method for Simulating Complex Fenestration Systems with Radiance against Field Measurements; submitted to Building Simulation 2017, International Building Performance Simulation Association, San Francisco, August 7-9, 2017.

Grobe, L.O, Wittkopf, S., Apian-Bennewitz, P., Jonsson, J.C., Rubin, M.D., 2010. Experimental validation of bidirectional reflection and transmission distribution measurements of specular and scattering materials, Proc. SPIE 7725, 772510.

Grobe, L.O., 2017a, Computational combination of the optical properties of fenestration layers at high directional resolution, Buildings 7 (22).

Grobe, L.O., Wittkopf, S., Kazanasmaz, Z.T., 2017b. High-resolution data-driven models of Daylight Redirection Components, J. Façade Design & Engineering, 5(2).

Jakubiec, J.A., Reinhart, C.F., 2011. DIVA-FOR-RHINO 2.0: Environmental parametric modeling in Rhinoceros/Grasshopper using Radiance, Daysim and EnergyPlus, Proceedings of Building Simulation 2011, Sydney, Australia.

Jonsson, J.C., Curcija, C., Wilson, H.R., Slack, J., Appert, S., Quinones, M., Zhao, S., Wu, K., Rubin, M., 2015. Measurement procedure for optical and thermophysical properties of fenestration shading fabrics to be used in WINDOW, LBNL Technical Report, October 1, 2015.

Kämpf, J.H., Scartezzini, J.-L., 2011. Ray-tracing simulation of complex fenestration systems based on digitally processed BTDF data, Proceedings of the CISBAT, Lausanne, Switzerland; pp. 349–354.

Kämpf, J.H., Paule, B., de Boer, J., Budde, E., Bueno, B., Geisler-Moroder, D., 2016. Advanced and future simulation tools, Technical report of Subtask T50-C5, International Energy Agency Solar Heating and Cooling Programme (IEA SHC) Task 50: Advanced Lighting Solutions for Retrofitting Buildings, 2016.

Klems, J.H., 1994a. A new method for predicting the solar heat gain of complex fenestration systems: I. Overview and derivation of the matrix layer calculation, ASHRAE Transactions 100 (1): 1065-1072.

Klems, J.H., 1994b. A new method for predicting the solar heat gain of complex fenestration systems: II. Detailed description of the matrix layer calculation, ASHRAE Transactions 100 (1): 1073-1086.

Kotey, N., 2009. Measurement and Models Related to Solar Optics in Windows with Shading Devices. PhD dissertation, University of Waterloo, 2009. https://uwspace.uwaterloo.ca/bitstream/handle/10012/4309/PhD%20Thesis%20Final_Nathan%20Kote.pdf?sequence=3&isAllowed=y, accessed June 8, 2017.

Krehel, M., Kämpf, J.H., Wittkopf, S., 2015. Characterisation and modelling of advanced daylight redirection systems with different goniophotometers; CISBAT 2015 International Conference on Future Buildings and Districts - Sustainability from Nano to Urban Scale, Lausanne, Switzerland, September 9-11, 2015, Vol. 1.

Lee, E.S., DiBartolomeo, D.L., Klems, J.H., Clear, R.D., Konis, K., Yazdanian, M., Park, B.C., 2009. Field Measurements of Innovative Interior Shading Systems for Commercial Buildings. ASHRAE Transactions 115(2): 706-728, 2009.

Lee, E.S., Thanachareonkit, A., Touzani, S., Dutton, S., Shackelford, J., Dickerhoff, D., Selkowitz, S., 2016. Technology Assessments of High Performance Envelope with Optimized Lighting, Solar Control, and Daylighting, Pacific Gas and Electric Company's Emerging Technologies Program, ET Project Number: ET14PGE8571.

Mardaljevic, J., 2000. Simulation of annual daylighting profiles for internal illuminance, Lighting Research and Technology 32(3): 111-118.

McNeil, A., 2011. On the sensitivity of daylight simulations to the resolution of the hemispherical basis used to define bidirectional scattering distribution functions, LBNL Technical deliverable, September 30, 2011, https://facades.lbl.gov/sites/all/files/2011-var-res-bsdf.pdf, accessed June 8, 2017.

McNeil, A., Lee, E.S., 2012. A validation of the Radiance three-phase simulation method for modelling annual daylight performance of optically complex fenestration systems. Journal of Building Performance Simulation (July): 1-14.

McNeil, A., 2013. The Five-Phase Method for Simulating Complex Fenestration with Radiance. https://facades.lbl.gov/sites/all/files/tutorial-fivephasemethod.pdf , accessed June 8, 2017.

McNeil, A., Jonsson, C.J., Appelfeld, D., Ward, G., Lee, E.S., 2013. A validation of a ray-tracing tool used to generate bi-directional scattering distribution functions for complex fenestration systems. Solar Energy 98 (2013): 404-414.

McNeil, A., Lee, E.S., Jonsson, J.C., 2017. Daylight performance of a microstructured prismatic window film in deep open plan offices; Building and Environment 2017, 113: 280-297; http://dx.doi.org/10.1016/j.buildenv.2016.07.019.

Microsoft, 2017. https://msdn.microsoft.com/en-us/library/6e3b887c.aspx, accessed June 8, 2017.

Molina, G., Bustamante, W., Rao, J., Fazio, P., Vera, S., 2015. Evaluation of Radiance's genBSDF capability to assess solar bidirectional properties of complex fenestration systems, Journal of Building Performance Simulation 8 (4): 216-225.

Noback, A., Grobe, L.O., Wittkopf, S., 2016. Accordance of Light Scattering from Design and De-Facto Variants of a Daylight Redirecting Component, Buildings 2016, 6(3), 30.

Radiance, 2010. *genBSDF*, https://radiance-online.org/learning/documentation/manual-pages/pdfs/genBSDF.pdf, accessed June 8, 2017.

Reinhart, C.F., Herkel, S., 2000. The simulation of annual daylight illuminance distributions — a state-of-the-art comparison of six RADIANCE-based methods, Energy and Buildings, 32 (2000): 167–187.

Reinhart, C.F., Walkenhorst, O., 2001. Validation of dynamic RADIANCE-based daylight simulations for a test office with external blinds, Energy and Buildings 33 (7) (2001): 683-697.

Roudsari, M.S., 2017. Honeybee[+] 0.0.3 Release notes for Grasshopper and Dynamo, posted August 23, 2017 at http://www.grasshopper3d.com/group/ladybug/forum/topics/honeybee-0-0-3-release-notes-for-grasshopper-and-dynamo, accessed August 30, 2017.

Saxena, M., Ward, G., Perry, T., Heschong, L., Higa, R., 2010. Dynamic Radiance – Predicting annual daylighting with variable fenestration optics using BSDFS, Fourth National Conference of IBPSA-USA, New York City, New York, August 11 – 13, 2010.

Schwanengel, C., 2010. Gegenüberstellung von Messtechniken zur Messung von Lichtstärkeverteilungen und Lichtstärkeverteilungsausschnitten, TechnoTeam Bildverarbeitung GmbH, August 2010, Table 3.1, page 34.

Schregle, R., Grobe, L.O., Wittkopf, S., 2015. Progressive photon mapping for daylight redirecting components, Solar Energy 2015 (114): 327–336.

Stover, J.C. Optical scattering: measurement and analysis. Bellingham: SPIE optical engineering press; 1995 May.

Tregenza, P.R., Waters, I., 1983. Daylight coefficients, Lighting Research and Technology, 15(2): 65-71.

Tzempelikos, A., Chan, Y.-C., 2016. Estimating detailed optical properties of window shades from basic available data and modeling implications on daylighting and visual comfort, Energy and Buildings 126: 396-407.

Ward Larson, G., Shakespeare, R., 1998. Rendering with Radiance: The Art and Science of Lighting Visualization. San Francisco: Morgan Kaufmann.

Ward, G., Mistrick, R., Lee, E.S., McNeil, A. Jonsson, J., 2011. Simulating the Daylight Performance of Complex Fenestration Systems Using Bidirectional Scattering Distribution Functions within Radiance. Leukos 7(4): 241-261.

Ward, G., Kurt, M., Bonneel, N., 2012. A Practical Framework for Sharing and Rendering Real-World Bidirectional Scattering Distribution Functions, LBNL-5954E, Lawrence Berkeley National Laboratory, Berkeley, CA, September 2012, https://eta.lbl.gov/sites/all/files/publications/lbnl12-tensor-tree-representation29102012.pdf, accessed June 8, 2017.

Ward, G., Kurt, M., Bonneel, N., 2014. Reducing anisotropic BSDF measurement to common practice, Proceedings of the Eurographics 2014 Workshop on Material Appearance Modeling: Issues and Acquisition, Lyon, France, June 25, 2014, pp. 5-8.

Wienold, J., Christoffersen, J., 2006. Evaluation methods and development of a new glare prediction model for daylight environments with the use of CCD cameras, Energy and Buildings 38(7):743–57.

Wienold J., 2016. evalglare version 2.0, September 2016, École Polytechnique Fédérale de Lausanne, https://www.radiance-online.org/community/workshops/2016-padua/presentations/211-Wienold-Evalgaare2.0.pdf, accessed June 8, 2017.

WINDOW 7, https://windows.lbl.gov/software/window/window.html, accessed June 8. 2017.